

**CATALYTIC MICROCHANNEL REACTORS
FOR CLEAN, INTRINSICALLY SAFE PROCESSES**

by

Mary Katharine Barillas

B.S. Chemical Engineering, Lafayette College, 2004

Submitted to the Graduate Faculty of
School of Engineering in partial fulfillment
of the requirements for the degree of
Master of Science in Chemical Engineering

University of Pittsburgh

2007

UNIVERSITY OF PITTSBURGH

SCHOOL OF ENGINEERING

This thesis was presented

by

Mary Katharine Barillas

It was defended on

November 27th, 2007

and approved by

Irving Wender, Professor, Department of Chemical and Petroleum Engineering

Robert M. Enick, Professor, Department of Chemical and Petroleum Engineering

Götz Vesper, Associate Professor, Department of Chemical and Petroleum Engineering

Copyright © by Mary Katharine Barillas

2007

CATALYTIC MICROCHANNEL REACTORS FOR CLEAN, INTRINSICALLY SAFE PROCESSES

Mary Katharine Barillas, M.S.

University of Pittsburgh, 2007

Chemically reacting flow occurs in many industrial settings such as combustion, catalysis, chemical synthesis, materials processing, etc. It is particularly important because of its function in catalysis, since catalysis accounts for 90% of the processes in the chemical industry. Catalytic processes with temperatures in the range of 400-1000 degrees C are classified as high temperature. Some industrially relevant high temperature catalytic processes include combustion and partial oxidation of hydrocarbons for energy production, and catalytic cracking for oil refining [1].

Microreactors, with characteristic dimensions less than one millimeter, have been shown to quench explosive reaction systems and are well worth exploring [2-5]. Microreactors have several advantages over conventional reactors, such as good thermal transport and increased surface-to-volume ratio. Microreactors can also be used to study explosive reaction systems such as hydrogen oxidation. Hydrogen oxidation is an important reaction for energy production through combustion and use in fuel cells. The reaction has wide flammability limits, 3-75 vol% of H₂ in air, and very high flame velocities which can lead to strong explosions [6]. In order to avoid explosions and to operate this reaction safely, it would be ideal to run hydrogen oxidation via the catalytic pathway.

The aim of this study is to investigate the use of microreactors for potentially explosive high temperature catalytic reactions through detailed numerical simulations, and the

development of a modular silicon microreactor. In this study, simulations will be performed using the same two-dimensional boundary layer model and CRESLAF module (version CHEMKIN 4.0 will be used). These simulation studies show the suppression of the homogeneous radical formation, which allows for the safe operation of the hydrogen oxidation reaction. An experimental microreactor was designed using detailed numerical simulations in Fluent. A preliminary experimental setup was also fabricated.

TABLE OF CONTENTS

PREFACE	XI
1.0 INTRODUCTION	1
1.1 PREVIOUS RESULTS	4
1.2 AIMS OF PRESENT STUDY	7
2.0 NUMERICAL SIMULATIONS	9
2.1 2-D BOUNDARY-LAYER SIMULATIONS	10
2.1.1 Reactor Model	12
2.1.2 Kinetic Model	12
2.1.3 Gas Phase Chemistry	13
2.1.4 Simulation Parameters and Numerics	13
2.1.5 Results and Discussion	14
2.2 3D NAVIER-STOKES SIMULATIONS	22
2.2.1 Reactor Model and Kinetics	23
2.2.2 Simulation Parameters and Numerics	25
2.2.3 Non-reactive mixing simulations	25
2.2.4 Reactive mixing simulations with homogeneous reactions	28
2.3 SUMMARY	32
3.0 EXPERIMENTAL	33

3.1	REACTOR DESIGN CONSIDERATIONS.....	33
3.2	MICROREACTOR CHIPS.....	36
3.3	CATALYST.....	37
3.4	REACTOR HOUSING/SETUP	38
3.5	EXPERIMENTAL MEASUREMENTS	40
3.6	HYDROGEN/AIR	40
3.7	HYDROGEN/OXYGEN	43
	3.7.1 Premixed	43
	3.7.2 Conclusions.....	48
4.0	FUTURE AND OUTLOOK.....	49
	4.1 NUMERICAL SIMULATIONS.....	49
	4.2 EXPERIMENTAL.....	50
	APPENDIX A.....	54
	APPENDIX B	61
	BIBLIOGRAPHY.....	64

LIST OF TABLES

Table 1. Compilation of high temperature reactions carried out in microreactors.	5
Table 2. Parameters tested and initial conditions.....	12
Table 3. Pre-exponentials and exponents for the heterogeneously dominated branch.	20
Table 4. Pre-exponentials and exponents for the homogeneously dominated branch.	21
Table 5. Initial/Boundary Conditions for Fluent Simulations.	25
Table 6. Mixing length produced at inlet angle	26
Table 7. Governing equations of the boundary layer model [42]	55
Table 8. Governing equations of the Navier Stokes model [43].....	56
Table 9. Gas phase kinetics for H ₂ -O ₂ Connaire [44].	57
Table 10. Surface reaction steps and rate parameters by Aghalayam et.al [45].	58
Table 11. Gas-phase kinetics of H ₂ – air mixture GRI[46].....	59

LIST OF FIGURES

Figure 1. Contour plot of the O ₂ (top row) and hydrogen radical (bottom row) mole fraction using Pt wall with a 1mm (left), 500 μm (middle) and 300 μm (right) microreactor diameters as a function of axial (z) and radial (r) distance at 1113K. [5]	7
Figure 2. Vesper et al. previous experimental setup [33].	8
Figure 3. A schematic overview the simulations program used to model the microreactor.....	11
Figure 4. Contour plot of the O ₂ (left) and hydrogen radical (right) mole fraction using Pt wall with a 300 μm microreactor diameters as a function of axial (z) and radial (r) distance at 1113K for various site densities.....	16
Figure 5. Plot of ignition distance as a function of site density, using Pt wall, 300 μm diameter at 1113K.....	17
Figure 6. Plot of ignition distance as a function of site density for 200 μm 300 μm and 400 μm diameters at 1113K.	19
Figure 7. Surface plot of the ignition distance based on the diameter and site density at 1113K.	19
Figure 8. Typical Gambit mesh.	23
Figure 9. Basic program structure for Fluent [43].....	24
Figure 10. Mixing as a function of inlet angle: Contour plot of hydrogen mole fraction with nozzle of 100 μm, at 1473K and H ₂ :O ₂ =1.....	26
Figure 11. Mixing as a function of nozzle size: Contour plot of hydrogen mole fraction with nozzle size of 50 μm (left) and 350 μm (right), both with inlet angle of 45 degrees, 1473K and H ₂ :O ₂ =1.	27
Figure 12. Mixing length as a function of nozzle size with inlet angle 45 degrees and nozzle depth 100 μm.	28

Figure 13. Homogeneous reactions and mixing as a function of nozzle size: Contour plot of hydrogen mole fraction (top) and water mole fraction (bottom) with nozzle size of 50 μm (left) and 350 μm (right), inlet angle of 45 degrees, at 1473K and $\text{H}_2:\text{O}_2=1$.	29
Figure 14. Conversion as a function of distance with nozzle size of 100 μm (red) and 350 μm (black), inlet angle of 45 degrees, at 1473K and $\text{H}_2:\text{O}_2=1$.	31
Figure 15. Microfabrication Procedure.	35
Figure 16. Image of microreactor.	37
Figure 17. Experimental Setup.	39
Figure 18. Contour plot of temperate raster using hydrogen/air at a power output of 55% at different hydrogen to oxygen ratios at a total flowrate of 20 sccm.	42
Figure 19. Contour plot of background temperature profile which corresponds to a power output of 55% and no flow.	43
Figure 20. Contour plot of temperate raster using hydrogen/oxygen at a power output of 55% at different hydrogen to oxygen ratios at a total flowrate of 20 sccm.	45
Figure 21. Conversion plot at different hydrogen to oxygen ratios at a total flowrate of 20 sccm at a power output of 55%.	46
Figure 22. Contour plot of temperate raster using hydrogen/oxygen at a power output of 55% at different flowrates keeping the hydrogen/oxygen ratio of 2.0.	47
Figure 23. Proposed re-design of reactor (a-c) top view (d) side view.	51

PREFACE

I would like to thank my advisor Dr. Götz Vesper for his support and the knowledge that I have gained.

I would also like to thank the members of my group: Tengfei Liu, Rahul Solunke, Tom Sanders, Michael Wartmann, Sudipta Chattopadhyay, Angie Noll, Janie Haven, Michaelangelo Tabone for their help, encouragement and support.

I would like to thank Sandy Hu for her help in learning microfabrication techniques in the JASMIN lab and Tim Fisher and Carsen Kline for their help at CMU Nanofabrication Facility.

Finally, I would like to thank my family, my friends, and Jeff for helping and encouraging me along the way.

1.0 INTRODUCTION

Chemically reacting flow is seen in many industrial settings such as combustion, catalysis, chemical synthesis, materials processing, etc. It is particularly important because of its function in catalysis, since catalysis accounts for 90% of the processes in the chemical industry. Catalytic processes with temperatures greater than in the range of 400-1000 degrees C are classified as high temperature. Some industrially relevant high temperature catalytic processes include combustion and partial oxidation of hydrocarbons for energy production, and catalytic cracking for oil refining [1].

Because these high temperature reactions occur under extreme conditions, it is important to understand how the process and reactions are affected by the changing process conditions. Ignition, the transition from the unreacted to the reacted state, has been studied for both the homogeneous and catalytic reactions [6, 7]. Heterogeneous (catalytic) ignition is desirable because it generally causes an increase in selectivity activity and yield; however, a catalyst complicates the study and understanding of the ignition behavior because it increases number of reaction pathways. Catalytic ignition generally occurs at lower temperatures and activation energies, and can prevent extreme temperatures. This in turn can prevent a loss in selectivity, flames or even explosions.

Microreactors have been shown to quench explosive reaction systems and are well worth exploring [2,3,4]. Microreactors are defined here as chemical reactors with characteristic

dimensions less than one millimeter [5]. Microreactors have several advantages over conventional reactors. Microreactors have high surface to volume ratios and small thermal masses which allows good control of thermal transport. The high surface to volume ratio also allows for large well defined catalytic surface areas. Because microreactors have good thermal transport, their use is particularly attractive for high-temperature catalytic reaction engineering. Catalytic reactions can be studied in microreactors with very good control and precision because of the well defined surface area and thermal transport. Also, microreactors are designed to be small and lightweight and are ideal for on demand production. Because of their small size and good control, they are ideal for use in combinatorial chemistry: because hundreds can easily be run in parallel. Also, because of the small volumes tested, new reaction regimes can be explored and research on potentially hazardous unknown reactions can be performed in microreactors in a safe matter.

Microreactors can also be used to study explosive reaction systems such as hydrogen oxidation. There is a current demand for alternative fuels and hydrogen is a potential alternative fuel because it is clean and efficient; however, the large scale use of hydrogen creates concerns over the safety of production, transportation and use. Hydrogen oxidation is an important reaction for energy production through combustion reaction and use in fuel cells. It is a very well understood and thoroughly tested reaction [8-11]. The reaction has wide flammability limits, 3-75 vol% of H₂ in air, and very high flame velocities which can lead to strong explosions [6]. This reaction is also strongly exothermic reaction ($\Delta H \approx -240$ kJ/mol). In order to avoid explosions and to operate this reaction safely, it would be ideal to run hydrogen oxidation via the catalytic pathway.

Typically, the study of this reaction system would have to be carried out under extreme conditions where it is very difficult to perform thorough studies. The hydrogen oxidation reaction is a chained, branched explosion when within the flammability limits and exposed to an ignition source. These branched explosions are characterized by a time delay whereby a radical pool is formed [12]. Because it has been found that surfaces act as radical capturers a large surface area would be needed to capture radicals and suppress the homogeneous reactions. Unlike conventional, large-scale reactors, microreactors have large-surface-to volume ratios and would provide the opportunity to study the extinction of the homogenous reactions through radical capturing.

1.1 PREVIOUS RESULTS

Over the past three decades, the miniaturization of reactor systems has increased due to the improvement of technologies that are used fabricate and analyze these systems. Numerous research groups have developed and studied micro-chemical systems. Different reactor configurations have been tested such as micro-mixers, micro-heat-exchangers, packed bed reactors, and laminated multi-channel reactors [13]. Table 1 includes a compilation of several high temperature reactions that have been carried out in microreactors. The contents and the format of the table were adapted and modified from Christine Apelee [14].

Table 1. Compilation of high temperature reactions carried out in microreactors.

Reaction type	Reaction	Catalyst	Max temp. reported (°C)	Reference	
Partial oxidation	Partial oxidation of methane $\text{CH}_4 + \frac{1}{2} \text{O}_2 \rightarrow \text{CO} + 2\text{H}_2$	Rh	700	15	
			1200	16	
	Epoxidation of ethane $\text{C}_2\text{H}_4 + \frac{1}{2} \text{O}_2 \rightarrow \text{C}_2\text{H}_4\text{O}$	Ag	250	17	
			300	18	
	Partial oxidation of propene to acrolein $\text{C}_3\text{H}_6 + \text{O}_2 \rightarrow \text{C}_3\text{H}_4\text{O} + \text{H}_2\text{O}$	CuO ₂	375	19	
	Partial oxidation of monomethylformamide to methyl-isocyanate $\text{CH}_3\text{HNCHO} + \frac{1}{2} \text{O}_2 \rightarrow \text{CH}_3\text{NCO} + \text{H}_2\text{O}$	Ag	300	20	
Oxidation	Methane Oxidation $\text{CH}_4 + 2\text{O}_2 \rightarrow \text{CO}_2 + 2\text{H}_2\text{O}$	Pt, Zr, V	450	21,22	
		Pt	520	23	
	Ammonia Oxidation $\text{NH}_3 + \frac{5}{4} \text{O}_2 \rightarrow \text{NO} + \frac{3}{2} \text{H}_2\text{O}$	Pt	650	24-29	
	Hydrogen Combustion $\text{H}_2 + \frac{1}{2} \text{O}_2 \rightarrow \text{H}_2\text{O}$	Pt	220	30	
				1000	32,33
		Pd	300	34	
			600	35	
Steam Reforming	Propane Reforming $\text{C}_3\text{H}_8 + 3\text{H}_2\text{O} \rightarrow 3\text{CO}_2 + 7\text{H}_2$	Ru	1000	36	
	Methanol-steam reforming $\text{CH}_3\text{OH} + \text{H}_2\text{O} \rightarrow \text{CO}_2 + 3\text{H}_2$	Pd, Cu	285	37	
	Isooctane-steam reforming $\text{C}_8\text{H}_{18} + \text{H}_2\text{O} \rightarrow 8\text{CO} + 17\text{H}_2$	Proprietary	670	38	
Nitration	Andrussov process $\text{CH}_4 + \text{NH}_3 + \frac{3}{2} \text{O}_2 \rightarrow \text{HCN} + 3\text{H}_2\text{O}$	Pt	1050	39	
Any reaction	Reactor design not for any particular reaction	Pt	700	40	
Ammonolysis	$4\text{NH}_3(\text{g}) + 3 \text{SiO}(\text{g}) \rightarrow \text{Si}_3\text{N}_4(\text{s}) + 3\text{H}_2\text{O}(\text{g}) + 3\text{H}_2(\text{g})$	-	1600	41	

It has been recently shown that the explosive nature of hydrogen oxidation can be reduced by using micro-machined reactors[2, 3, 11]. Numerical simulations were previously done by Sudipta Chattopadhyay to differentiate the influences of the heterogeneous and homogeneous reaction pathways in the hydrogen oxidation reaction system [5]. She incorporated the homogeneous and heterogeneous pathways in the two dimensional boundary layer CRESLAF model using CHEMKIN 3.1. From these results the effect of reactor diameter on ignition behavior was studied and can be seen in Figure 1. The mole fractions of hydrogen (H) radicals and O₂ are seen in the contour plots. From the O₂ contour plot it can be seen that the O₂ is immediately consumed at wall surface, due to the catalyst. As can be seen in the 1mm diameter case, a buildup of H radicals is needed before the immediate consumption of O₂ can be completed. Since H radicals are a strong indicator of homogeneous reactions, these results indicate that the ignition behavior is strongly influenced by homogeneous reactions. As the reactor diameter gets smaller (500 micrometers) the H radical concentration drops by 5 orders of magnitude and the O₂ contour plot shows a broadening of the concentration profile. This broadening indicates that the O₂ has a chance to diffuse to the catalyst wall and is being consumed by the catalyst. This suggests a weakening of the homogeneous reaction. At even smaller diameters (300 micrometers) the disappearance of H radicals is seen, indicating that the homogeneous reactions have been quenched.

Veser et al. have also developed a simple microreactor system for high temperature microreactor studies (See Figure 2). It consists of two silicon wafers pressed together with a platinum wire which acted as both the catalyst and the heater. Initially these wafers were housed in a stainless steel housing as seen in Figure 2 which were later changed to ceramic blocks.

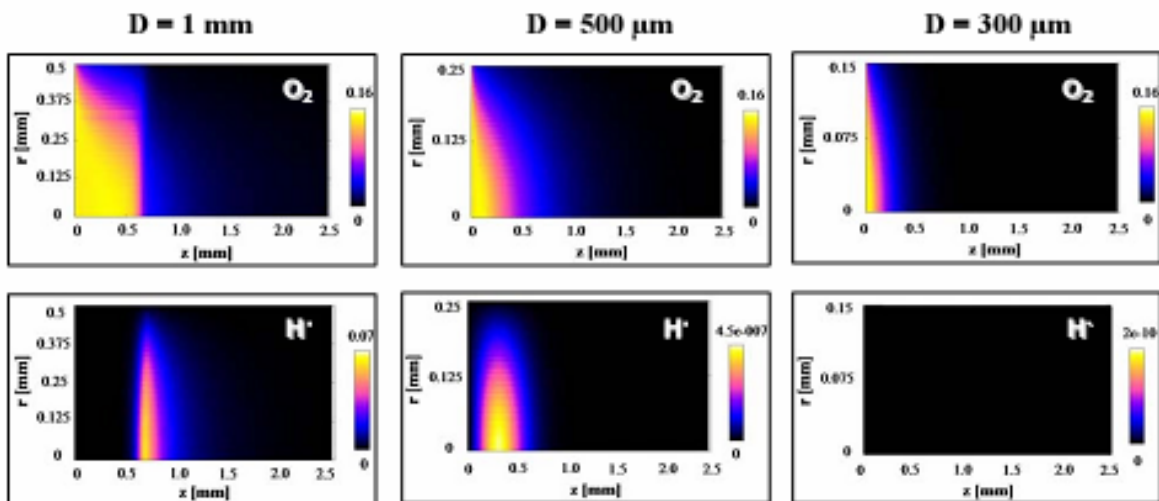


Figure 1. Contour plot of the O₂ (top row) and hydrogen radical (bottom row) mole fraction using Pt wall with a 1mm (left), 500 μm (middle) and 300 μm (right) microreactor diameters as a function of axial (z) and radial (r) distance at 1113K. [5]

1.2 AIMS OF PRESENT STUDY

The aim of this study is to investigate the use of microreactors for high temperature catalytic reactions that have potentially explosive nature through detailed numerical simulations and the development of a modular silicon microreactor. In this study, simulations will be performed using the same two-dimensional boundary layer model and CRESLAF module; however, CHEMKIN version 4.0 will be used. The objective of these simulation studies is to identify the cause of the inhibition of the homogeneous reactions and discover under what reactor dimensions would the quenching of explosions be the greatest. After performing detailed numerical simulations, an experimental microreactor will be designed. The development of the experimental setup will also be discussed.

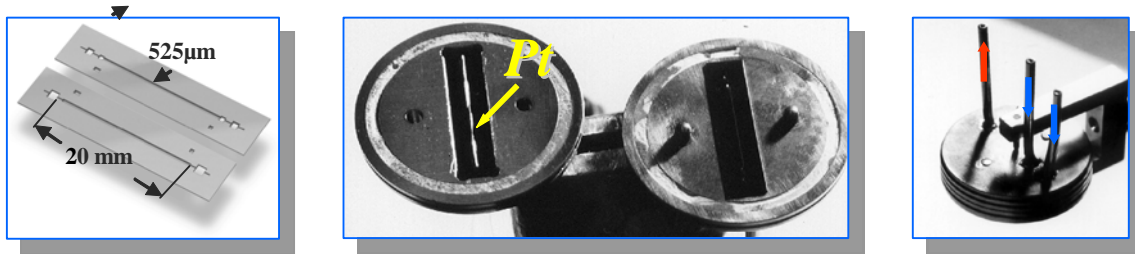


Figure 2. Vesper et al. previous experimental setup [33].

Chapter 2 discusses the results of modeling hydrogen oxidation in a microreactor using a boundary layer model and the full Navier-Stokes equations. This chapter also includes a detailed description of the kinetic and reactor model used in both cases. Chapter 3 covers the development of a microreactor which will be used to verify the numeric modeling results, and Chapter 4 discusses the future and outlook of this project along with a list of improvements that can be made on the microreactor.

2.0 NUMERICAL SIMULATIONS

There are several options for modeling reactive flow. In this study we have chosen to study ignition behavior of hydrogen oxidation using two models: the boundary layer model in CHEMKIN and the Navier-Stokes equations solved using FLUENT. There are several conditions that need to be considered before choosing the numerical model which include the flow conditions, accuracy of the results, and the computational expense. The two models will be used to model the reactive flow in a catalytic microreactor under high temperature conditions. These models include convective and diffusive mass transport.

Generally there are three model choices for modeling reactive flow: Navier-Stokes, boundary layer model, and plug flow. Solving the complete Navier-Stokes equations is the most comprehensive model and the most computationally expensive option, whereas the plug flow model is the least comprehensive. The intermediate option is using the boundary layer model which assumes no axial diffusive transport, but focuses on the transport to and from the walls, which is important when trying to study the interplay between homogeneous and heterogeneous reactions.

2.1 2-D BOUNDARY-LAYER SIMULATIONS

The hydrogen oxidation reaction will be studied using a 2-D boundary layer model in Chemkin. This particular model accounts for radial diffusion and the conservation of species, mass and energy. Convection is assumed to be dominant in the axial direction along the channel and axial diffusion is neglected. The CHEMKIN model used is the cylindrical channel shear-layer flow reactor (CRESLAF) and the method of use is seen in Figure 3. This model couples fluid flow, gas-phase chemistry, and surface chemistry in a laminar-flow channel. The model predicts gas-phase temperature, velocity fields, concentration fields, and surface species coverage. Results are calculated based on the initial and boundary conditions such as surface temperature, flow-rate, partial and total pressures, and reactor dimensions. The range of values tested is seen in Table 2. A sample input file can be found in Appendix A

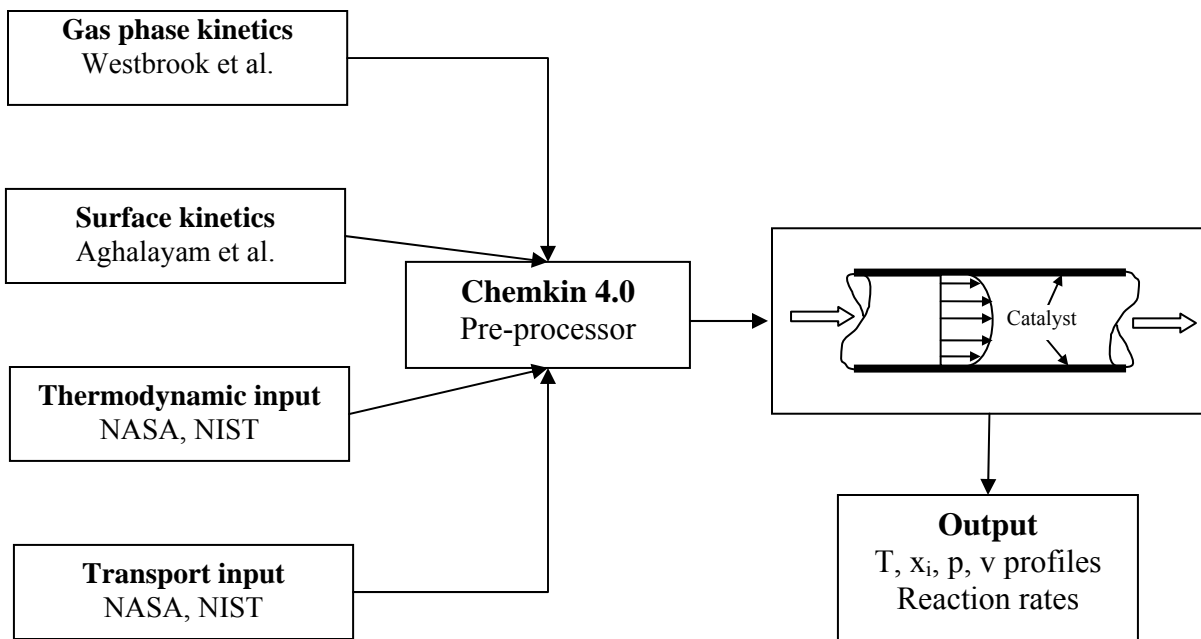


Figure 3. A schematic overview the simulations program used to model the microreactor.

Table 2. Parameters tested and initial conditions.

Parameters Tested	
Temperature (K)	1113
Inlet flowrate (m/s)	9
Total Pressure (atm)	1
Site Density (Pt/cm ²)	0-2.71e-9

2.1.1 Reactor Model

The characteristic features of our model are high velocities, keeping the Peclet number much larger than 1 which ensured convective dominant flow. Small dimensions were also used which kept the flow laminar. Diffusive heat and mass transport were only allowed in the radial direction.

2.1.2 Kinetic Model

To study the ignition behavior and the reason for quenching we used detailed elementary reaction mechanisms for the homogeneous reaction mechanism and the surface reaction mechanism over Pt. We wanted to determine if the catalytic reactions are so fast that they consume the reactants before the homogeneous radical pool can be built up or if the catalytic surface was acting as a radical capturer, capturing and limiting the amount of radicals formed in

the gas phase. We can distinguish between these mechanisms by varying the amount of catalyst loading which weakens the catalytic activity.

2.1.3 Gas Phase Chemistry

These numerical simulations used the Westbrook gas phase mechanism given in Appendix A, Table 9. This mechanism is a list of elementary chemical reactions and associated rate constant expressions. This detailed chemical reaction mechanism is optimized to represent hydrogen flame chemistry. It consists of 8 species and 21 reactions. An inert surface was also simulated; however, this is an idealized situation which can be realized only computationally. This surface is used as a reference case in our study.

To correctly identify the interplay between homogeneous and heterogeneous reactions, a surface mechanism which contains all possible reactions, reactant and intermediates was used. The catalytic wall used was platinum and the mechanism was obtained from Aghalayam (see Appendix A). Aghalayam et al. used sensitivity analysis to find kinetic parameters, optimized the pre-exponential factors, and also included the adsorbate-adsorbate interaction on activation energies. In the mechanism, Pt(S) indicates a free Pt surface site and species followed by (S) denote adsorbed species. The site density of the Pt surface is varied from 0 to $2.71 \cdot 10^{-9}$ mol/cm², where zero corresponds to the purely homogeneous inert case.

2.1.4 Simulation Parameters and Numerics

The reactor was modeled as an axis-symmetric tubular reaction channel. The pressure was maintained at one bar, gas inlet velocity was 9 m/s, and reactants were a stoichiometric mixture

of premixed hydrogen in air. The channel diameter was varied between 1 mm and 50 μm . The reactant length was adjusted to observe ignition. The surface temperature was maintained at 1113K. Other temperatures were tested but will not be mentioned in this work because they showed similar trends. The temperature was chosen because it was previously shown that at this temperature, the reactions in the majority of the reactor diameters were heterogeneously dominated. The only variable tested in this reactor study was the surface site density.

The simulations were performed on an Intel processor 3.2 GHz, utilizing 40-100 mesh points in radial direction with non-uniform grid point distribution of 1.2 indicating that the nodes are more concentrated near the wall. The program automatically adapts the grid in the axial direction to achieve the specified numerical accuracy, which was set to at least $1\text{e-}4$. Typical integration times varied between 1 to 3 minutes for a single run.

2.1.5 Results and Discussion

Previous results showed that we could quench homogeneous reactions in a sufficiently small reactor simply by adding catalyst; however it is important to identify whether the fast catalytic reactions are consuming the reactants before the homogeneous radical pool can be built up or if the catalytic surface is acting as a radical capturer, capturing the radicals and limiting the amount of radicals formed in the gas phase. By varying the catalyst loading, the catalytic activity is weakened and it becomes possible to distinguish between these two hypotheses.

The contour plots of the oxygen and hydrogen mole fractions are shown in Figure 4. The top contour plot corresponds to a completely covered Pt surface, the bottom contour plots correspond to the purely homogenous case with no catalytic reactions, and the middle plot corresponds to a case with less than 1% catalyst coverage. In the top plots it can be seen that a

negligible amount of H radicals are formed indicating that the homogeneous reactions are not taking place. In the homogeneous case, again it can be seen that the consumption of the O₂ does not occur until the hydrogen radical pool has been formed. The intermediate case shows that the catalytic reaction has been extremely weakened because the reaction front has been significantly increased from 0.2 mm to 5 mm. Also in this case the homogeneous reactions are still not taking place. If the fast catalytic reactions were the driving force one would expect a buildup of the radical pool and a slight increase in the ignition distance; however, since we still do not see a buildup of the radical pool and the ignition has been greatly increased, we can attribute the quenching behavior to the wall behaving a radical capturer.

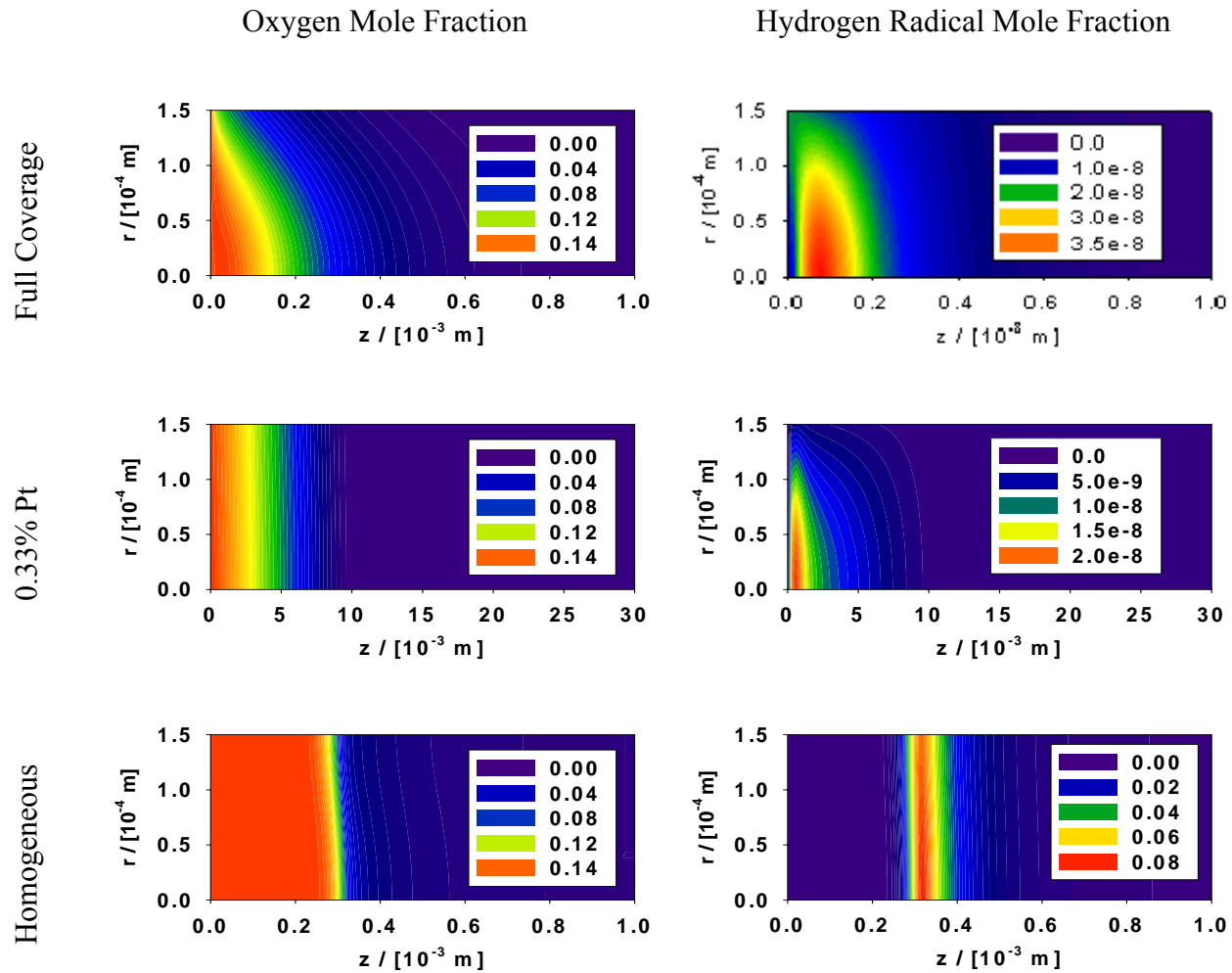


Figure 4. Contour plot of the O₂ (left) and hydrogen radical (right) mole fraction using Pt wall with a 300 μm microreactor diameters as a function of axial (z) and radial (r) distance at 1113K for various site densities.

To quantify the results an ignition distance or delay has been chosen. This ignition distance will be defined as the distance along the centerline of the reactor at which 50% of the hydrogen has been converted.

When a catalyst is incorporated into a reactor it is expected that the ignition distance would gradually increase as the site density (number of wall capturers) is decreased (as seen in red dashed line in Figure 5). However, what we actually find is that as the catalyst loading is decreased there is an initial increase in the ignition distance until a maximum is reached where a further decrease in catalyst loading results in a decrease in the ignition distance. This decrease is due to the homogeneous reactions beginning to kick in. From the plot seen in Figure 5 we have turned platinum usually thought of as an ignition promoter into a reaction inhibitor.

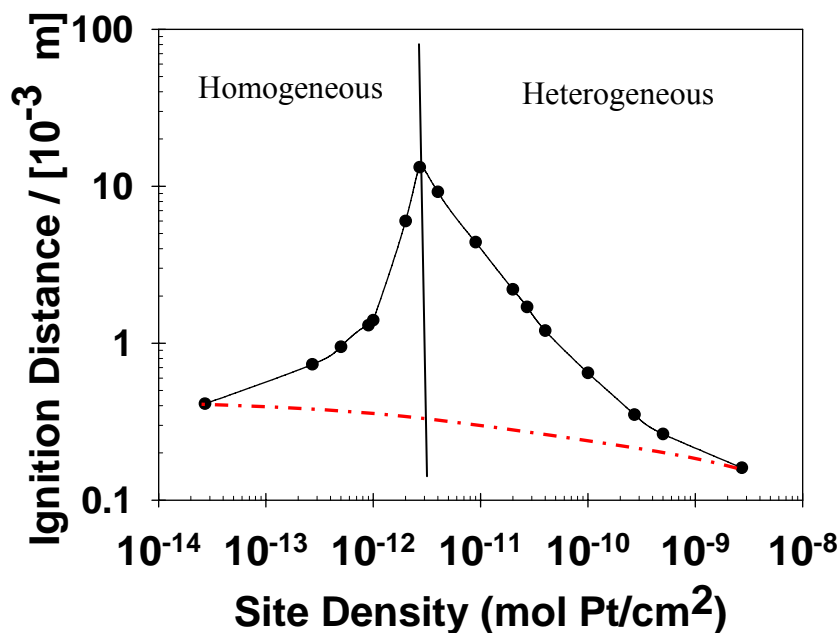


Figure 5. Plot of ignition distance as a function of site density, using Pt wall, 300 μm diameter at 1113K.

Figure 6 shows a plot of the ignition distance for three different diameters versus site density. It can be seen that the maximum ignition distance is inversely proportional to the diameter. Also the site density for the maximum ignition distance shifts to lower site densities. It is known that the surface to volume ratio increases as the diameter is decreased and therefore the maximum ignition distance probably corresponds to the same catalytic surface area. Figure 7 is a surface plot, which includes all diameters run, which shows the overall ignition behavior. It can be seen that the maximum ignition occurs at the smallest diameter and that at this point the ignition distance has been increased to about 4 centimeters due to the radical capturing of the Pt wall.

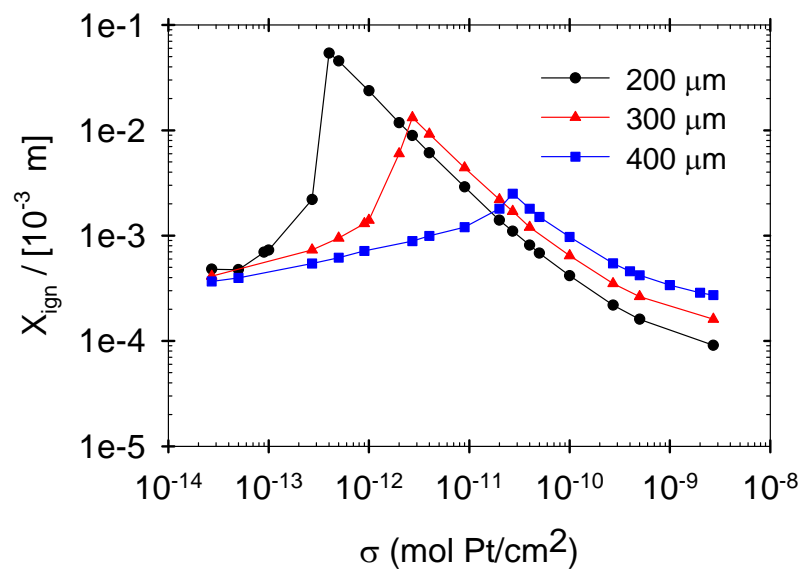


Figure 6. Plot of ignition distance as a function of site density for 200 μm 300 μm and 400 μm diameters at 1113K.

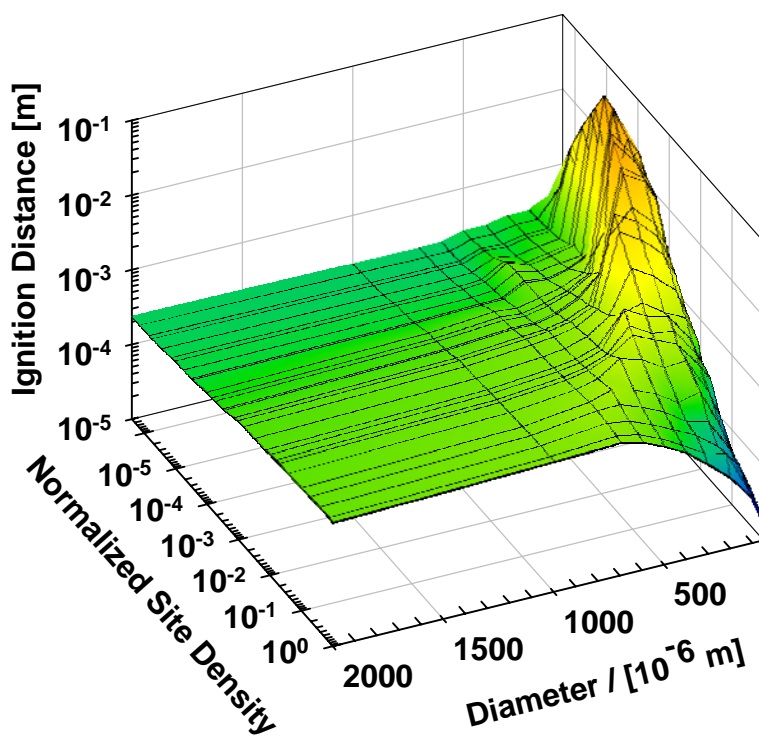


Figure 7. Surface plot of the ignition distance based on the diameter and site density at 1113K.

A mathematical fit was conducted to find a generalized formula to describe this ignition behavior, so that an ignition distance can be predicted depending on the diameter and site density. From Figure 5, it can be seen that there are two distinct regions that need to be fit: the left side of the curve is considered homogeneously dominated and the right had side of the curve is considered heterogeneously dominated. The homogeneously and heterogeneously dominated curves were independently fit using a double power law equation where the sum squared residuals were minimized (as seen in Equation 1). This fit provides predictive information about the maximum ignition distance and the corresponding site density for any given diameter.

$$X_{ign} = a_1 + \sigma^{b_1} + a_2 + \sigma^{b_2} \quad \mathbf{1}$$

Table 3. Pre-exponentials and exponents for the heterogeneously dominated branch.

Diameter (mm)	a ₁	b ₁	a ₂	b ₂
50	2.05E-06	-1.000	1.55E-05	0
100	5.87E-08	-1.000	7.81E-07	0
200	7.79E-06	-1.000	9.51E-05	0
300	1.57E-05	-1.000	1.63E-04	0
400	2.25E-05	-1.000	2.78E-04	0

Table 3 shows the results of the fitting for the heterogeneously dominated branch. From the fitting it was determined that the second exponent was not necessary to minimize the residuals and as a result the second exponent drops out or becomes zero. Also it can be seen that the ignition behavior is inversely proportional to the site density which makes sense in the

heterogeneously dominated branch, because as the site density decreases there are fewer sites for the catalytic recombination of radicals and the ignition distance would increase.

Table 4 shows the results of the fitting for the homogeneously dominated branch. Initially it can be seen that the second exponent starts off at zero and becomes nonzero as the diameter increases, which is an indication of the strengthening of the homogeneous reactions. For the first exponent (b_1) the ignition distance is dependent on the square of the site density which indicates that the homogeneous ignition is sensitive to the presence of the catalyst. As we increase the diameter to 400 μm it can be seen that the value of b_1 decreases significantly which corresponds to the fact that at larger diameters the effect of the catalyst wall becomes weaker simply because it has become farther from the reference point which is defined along the centerline of the reactor.

Table 4. Pre-exponentials and exponents for the homogeneously dominated branch.

Diameter (mm)	a1	b1	a2	b2
50	2.52E+08	2.01	3.23E-04	0
100	8.52E+08	2.00	2.52E-04	0
200	1.99E+05	2.02	4.37E-04	0
300	1.00E+04	2.00	1.00E-03	3.30E-02
400	1.00E-04	0.50	6.19E-03	2.70E-01

2.2 3D NAVIER-STOKES SIMULATIONS

Because the 2D boundary layer model previously shown is limited to reactors in which the flow is convectively dominant, and also the model assumed completely premixed conditions, it is important to show that the quenching of the homogeneous reactions could occur using a more realistic model. Fluent 6.1, a commercially available computational fluid dynamics program, was used to create the three dimensional realistic model of the hydrogen oxidation system in a microreactor. This program was used to solve the complete set of Navier-Stokes equations.

Because of the small dimensions that were needed to quench the homogeneous reactions, the flow through the reactor is laminar. Having laminar flow is a problem because the mixing has to occur mostly through diffusion processes which are generally slow. Because these simulations were also going to be used as the first step in designing a high temperature microreactor, it was important to use these simulations to find a microreactor that not only quenches homogeneous reactions, but also has good mixing.

The initial design considerations for a microreactor that will ultimately quench homogeneous reactions included designing a reactor that would have two inlets and one outlet. This would guarantee that there was no premixing or reactions prior to reaching the reactor channel. The two inlets would meet at a nozzle, which shortens the diffusion length and increases the mixing characteristics of the reactor (See Figure 8).

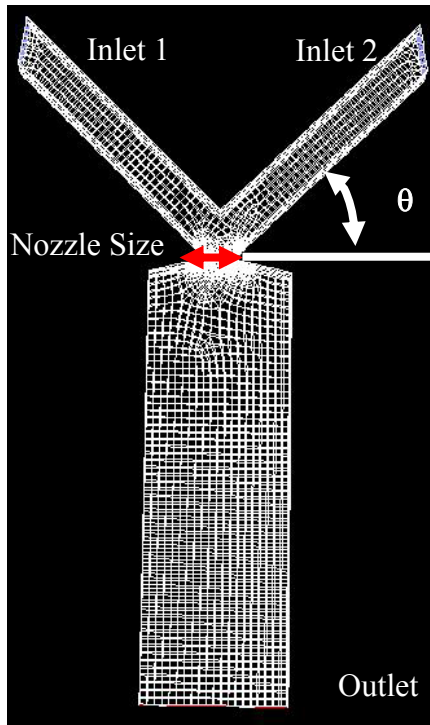


Figure 8. Typical Gambit mesh.

2.2.1 Reactor Model and Kinetics

The reactor model that will be used is the species and transport and reacting flow models within Fluent. The solver used was the segregated, three dimensional, double precision solver, because of the complexity of the geometry, incompressible flows, and stiff system of equations. The flow conditions will be the same as that mentioned in the boundary layer model; however, the reactor geometries tested will be significantly different. The reactor geometry will be more realistic with non-premixed conditions. Fluent solver requires three major inputs which include the results from the preprocessing program (Gambit, TGrid, etc.), identification of the materials

that will be used, and finally the initial and boundary conditions. The structure of the Fluent program can be seen in Figure 9.

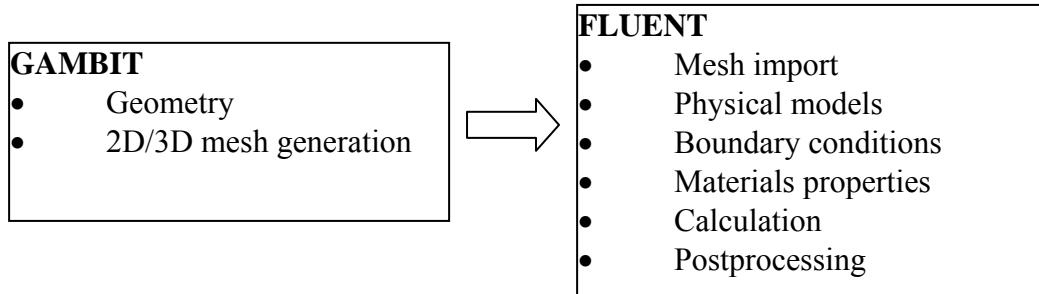


Figure 9. Basic program structure for Fluent [43]

There were several choices of how to input the geometry into Fluent, but the easiest and most versatile was Gambit. Gambit is a preprocessing program which creates the geometry and mesh to be used in Fluent. Figure 8 shows a mesh that was created by Gambit.

The Fluent database provides all the transport and thermodynamic properties needed to solve the problem. The reactor initial and boundary conditions are shown in

Table 5. The solver then uses these three major inputs to solve the mass, momentum and energy equations seen in Equations (8-12) seen in Appendix A. The GRI mechanism was used for the gas phase chemistry kinetics. This mechanism can be seen in Appendix A, Table 11.

2.2.2 Simulation Parameters and Numerics

Only homogeneous reactions were included because of the computational expenses that were required to solve the Navier Stokes equations and the stiff reactor kinetics. Each simulation took about two days; however, there were several ways to decrease the simulation time which includes solving the flow conditions first and then turning on the reactions, also having a significantly small mesh helped decrease computational times. The tolerances were set to $1e-6$ for the continuity and momentum equations and $1e-3$ for the individual species equations. The energy equation was deactivated to run the reactor isothermally.

Table 5. Initial/Boundary Conditions for Fluent Simulations.

Inlet Velocity	Inflow, 9 m/s
Temperature	1473 K
Mole fractions	Inlets: $H_2=1$, $O_2=1$
Pressure	1 atm
Outlet	Outflow

2.2.3 Non-reactive mixing simulations

Since we wanted to design a reactor that had the best mixing conditions, we chose to test several parameters to identify a reactor which could be tested further, experimentally. The parameters varied were the inlet angle and the nozzle size.

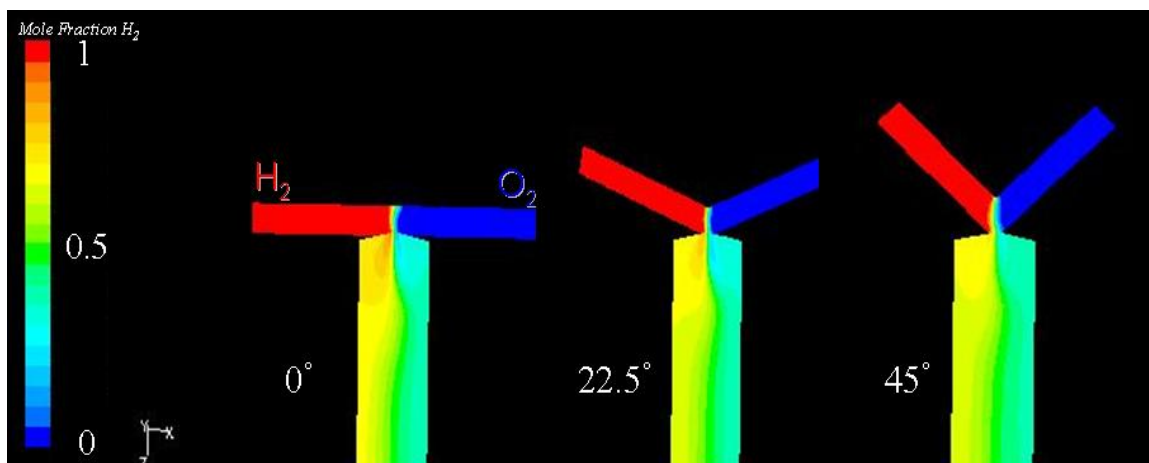


Figure 10. Mixing as a function of inlet angle: Contour plot of hydrogen mole fraction with nozzle of 100 μm , at 1473K and $\text{H}_2:\text{O}_2=1$.

The effect of the varying inlet angle can be seen in Figure 10. Qualitatively there appears to be no significant difference between the mixing lengths of these three different geometries. To quantify the mixing quality of the reactors, a mixing length was defined. It is defined as the point in the microchannel when the mole fraction of hydrogen was within 10% of the perfectly mixed state value of 0.5 across the reactor channel. The effect of the inlet angle on mixing can be seen in Table 2: as the inlet angle is varied the mixing length is shortest for the inlet angle zero.

Table 6. Mixing length produced at inlet angle.

Inlet Angle ($^\circ$)	Mixing length (cm)
0	1.04
22.5	1.24
45	1.82

The nozzle size was also varied to see its effect on the mixing length. Figure 11 shows the contour plots of the hydrogen mole fraction for two reactors with inlet angles of 45 degrees.

It can be seen that the mixing is better in the reactor with the smaller nozzle. This is expected because the diffusional path has been significantly decreased in this area. The mixing length was also quantified and the results can be seen in Figure 12. The results indicate that as the nozzle size is increased the mixing length is also increased, although less dramatically as the nozzle size becomes greater than 200 micrometers. This is expected because decreasing the nozzle size decreases the diffusion length and increases the mixing in these nozzles and would increase the amount of mixing in the laminar flow regime.

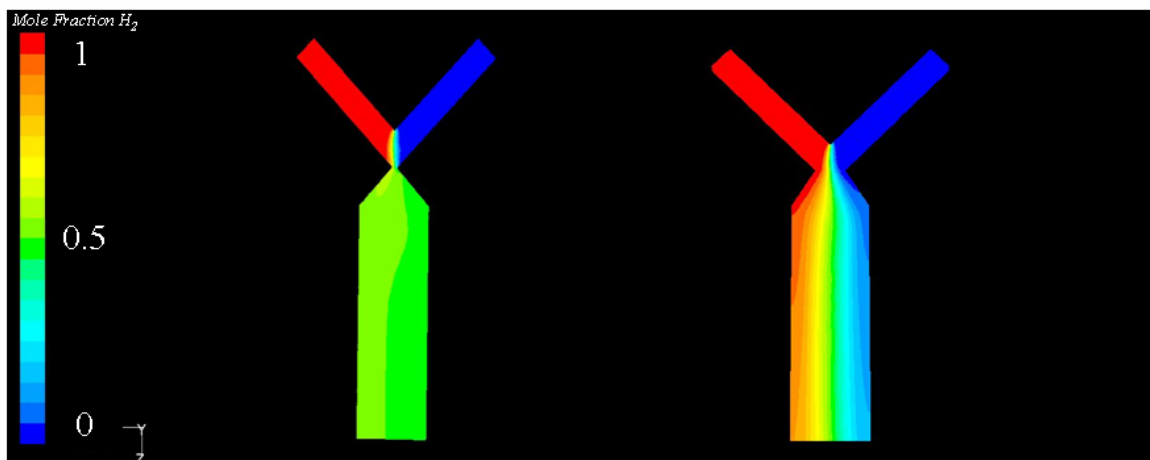


Figure 11. Mixing as a function of nozzle size: Contour plot of hydrogen mole fraction with nozzle size of 50 μm (left) and 350 μm (right), both with inlet angle of 45 degrees, 1473K and $\text{H}_2:\text{O}_2=1$.

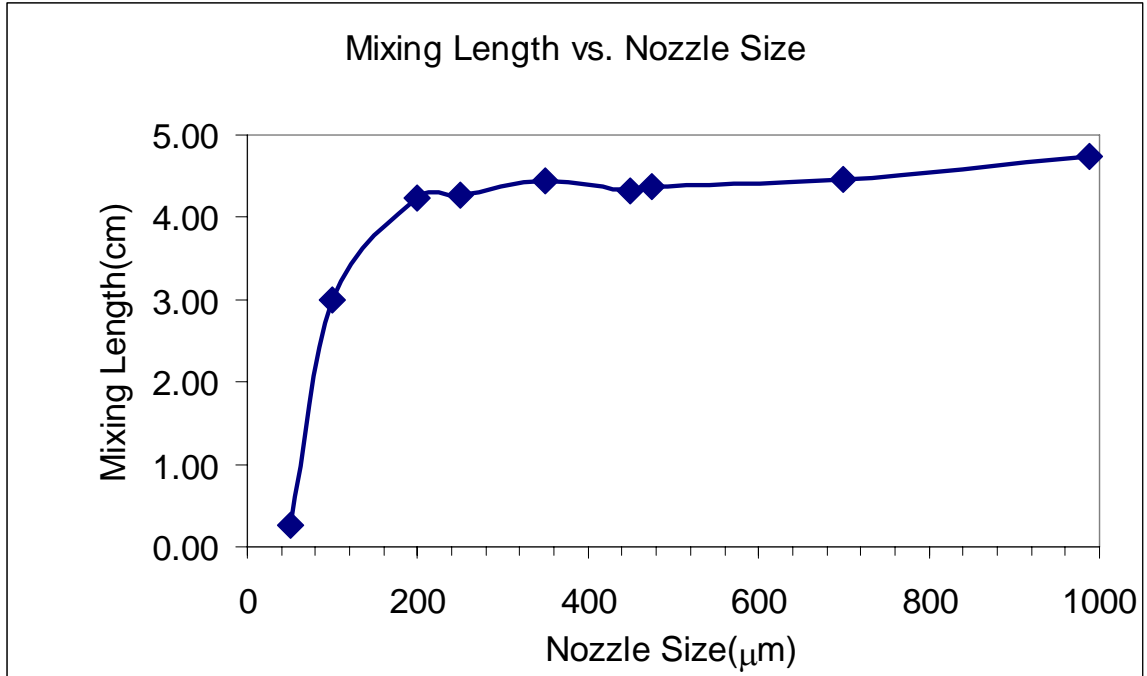


Figure 12. Mixing length as a function of nozzle size with inlet angle 45 degrees and nozzle depth 100 μm.

2.2.4 Reactive mixing simulations with homogeneous reactions

Since not only pure mixing will be occurring within the reactors it is important to see what kind of effect the reactions will have on the mixing. In Figure 13, the top contour plots show the hydrogen mole fraction of two reactors with significantly different mixing lengths. It can be seen that the reactor on the left shows homogeneous mixing whereas the reactor on the right shows very little mixing except along the interface of hydrogen and oxygen. It is necessary to determine if the homogeneity of the reactor will be worsened with the incorporation of homogeneous reactions or if the mixing length limits the conversion.

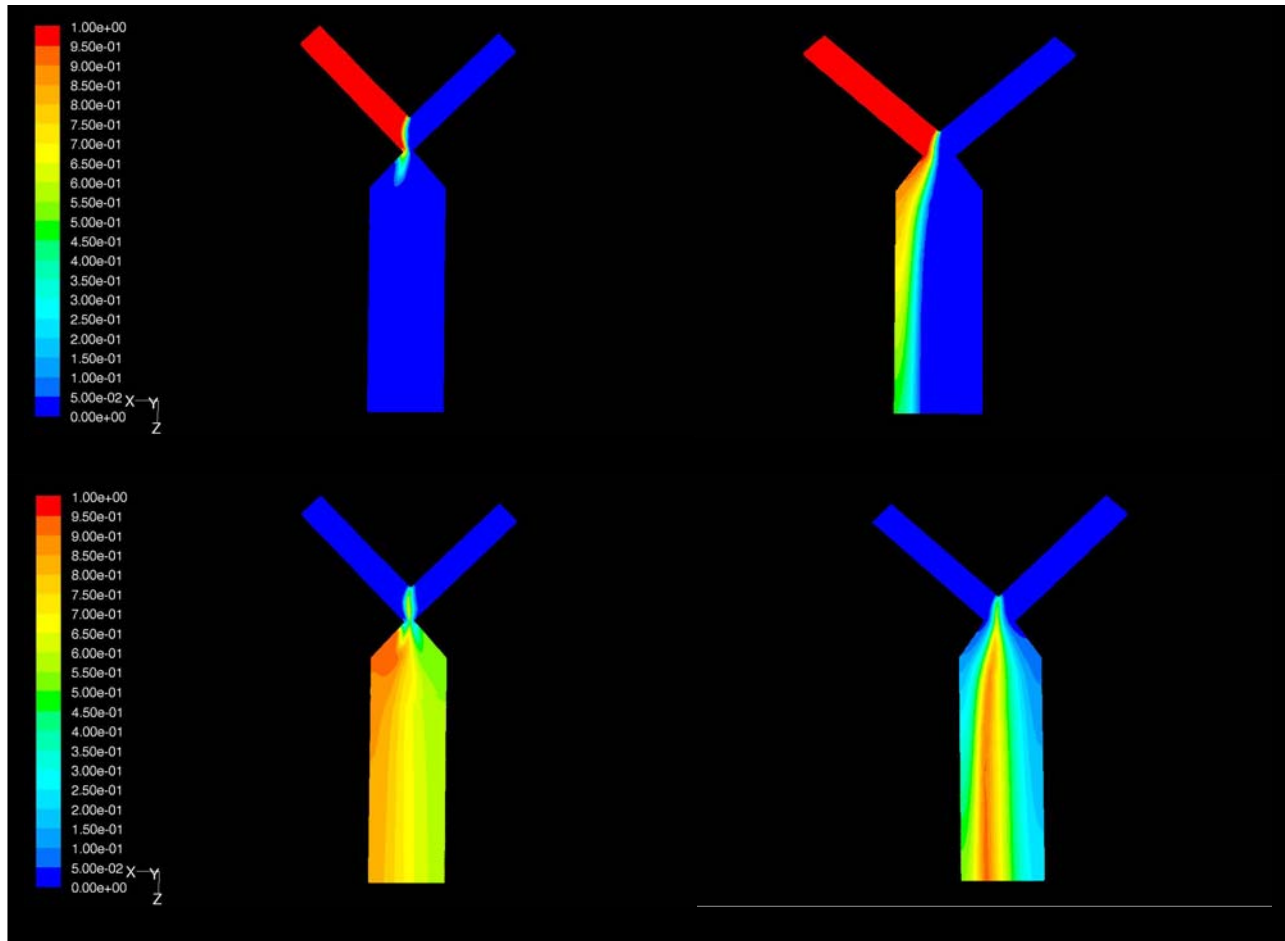


Figure 13. Homogeneous reactions and mixing as a function of nozzle size: Contour plot of hydrogen mole fraction (top) and water mole fraction (bottom) with nozzle size of 50 μm (left) and 350 μm (right), inlet angle of 45 degrees, at 1473K and $\text{H}_2:\text{O}_2=1$.

It can be seen in Figure 13 that complete conversion is obtained in the well mixed case and has not been achieved in the poorly mixed case. Qualitatively, it can be seen that the reactive length is shorter than the mixing length for the well mixed case as compared to Figure 11. The reaction in this case also seems to be very homogeneous. The poorly mixed case shows non-homogeneity in the reactor and has not reached complete conversion.

To quantify the results, it was necessary to develop a method to calculate the conversion in the reactor. The conversion was calculated using molar flowrates. To get the molar flowrates, an area-weighted average of the molar concentration, density and mass flowrate were used. The conversion was calculated using Equations 2 and 3.

$$F\left(\frac{kmol}{s}\right) = \frac{m\left(\frac{kg}{s}\right) * C_{H_2}\left(\frac{kmol}{m^3}\right)}{\rho\left(\frac{m^3}{kg}\right)} \quad 2$$

$$Conversion = 1 - \frac{F_{H_2,final}}{F_{H_2,initial}} \quad 3$$

It can be seen in Figure 14 that conversion in the well mixed reactor (red dots) indicates that 100% conversion can be achieved with a nozzle size of 100 um, whereas less than 100% conversion is achieved in the reactor with a nozzle size of 350 um. The mixing has been improved due to reactions which could be attributed to the gradient for diffusion processes in this area of the induced flow caused by the reduction in the total the number of moles for hydrogen oxidation.

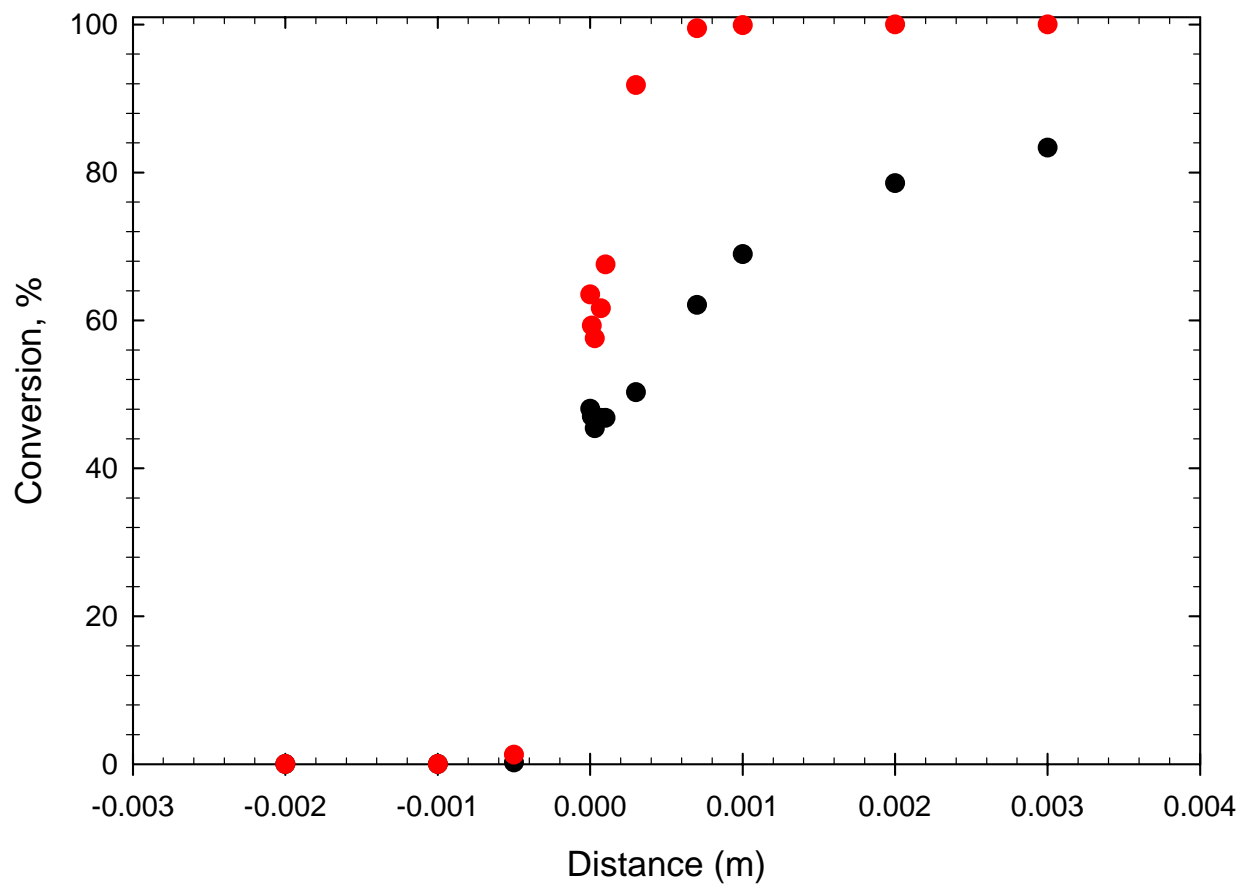


Figure 14. Conversion as a function of distance with nozzle size of 100 μm (red) and 350 μm (black), inlet angle of 45 degrees, at 1473K and $\text{H}_2:\text{O}_2=1$.

2.3 SUMMARY

With the use of reactive modeling we were able to determine that quenching in a microreactor is due to the catalyst acting as a radical capturer. Also it was found that the platinum could act as both a promoter and an inhibitor in the hydrogen oxidation reaction. When using a complex reactor geometry, the results showed that having reactions actually induces mixing in the reactor. Since we determined that the mixing distance was on the order of a few millimeters in most reactors, we created an initial microreactor design which will be discussed further in the next chapter.

3.0 EXPERIMENTAL

Because of the many advantages of microreactors which have already been mentioned, the following study will use a microreactor as a tool to study high temperature catalytic reactions. The reactor design and fabrication will be discussed, as well as preliminary studies on hydrogen oxidation in air and pure oxygen.

Developing a microreactor that is both easy to fabricate, setup and use and is stable over a wide range of operating conditions is a significant challenge. There is also the desire to reuse all of the parts and make them interchangeable to ensure a modular reactor design. There are several options to consider when deciding how to fabricate the reactor. These options include dry etching, soft lithography, wet etching, and laser ablation, among others. Silicon etching techniques were chosen because they are readily available at the JASMIN microfabrication laboratory at the University of Pittsburgh and also at Carnegie Mellon's Nanofabrication facility. The facilities at these laboratories provide all the necessary tools to do photolithography and DRIE etching.

3.1 REACTOR DESIGN CONSIDERATIONS

Since some key parameters have been identified to the design of the microreactor (eg. nozzle size and inlet angle), it is important to test these numerical results using experiments. The first step is

to fabricate the microreactor. The microreactor will be fabricated on a (100) Si wafer using deep reactive ion etching (DRIE). DRIE is used here over wet-etching because wet-etching has isotropic etching patterns and the complex geometry will significantly increase the complexity of the mask design. Figure 15 shows the complete microfabrication procedure which starts from a 4 inch (100) silicon wafer (University Silicon) which has 1 μm thermally grown silicon oxide. A mask is created on a 4'' Si (100) substrate with a 1 μm SiO₂ layer through photolithography. The SiO₂ mask is then etched using BOE (buffered oxide etching) to be used in DRIE-ICP. An STS Induced Couple Plasma Deep Reactive Ion Etcher using the gases C₄F₈, SF₆, Ar, O₂, N₂, and He was used to etch for 3 hours to achieve a depth of 250 μm .

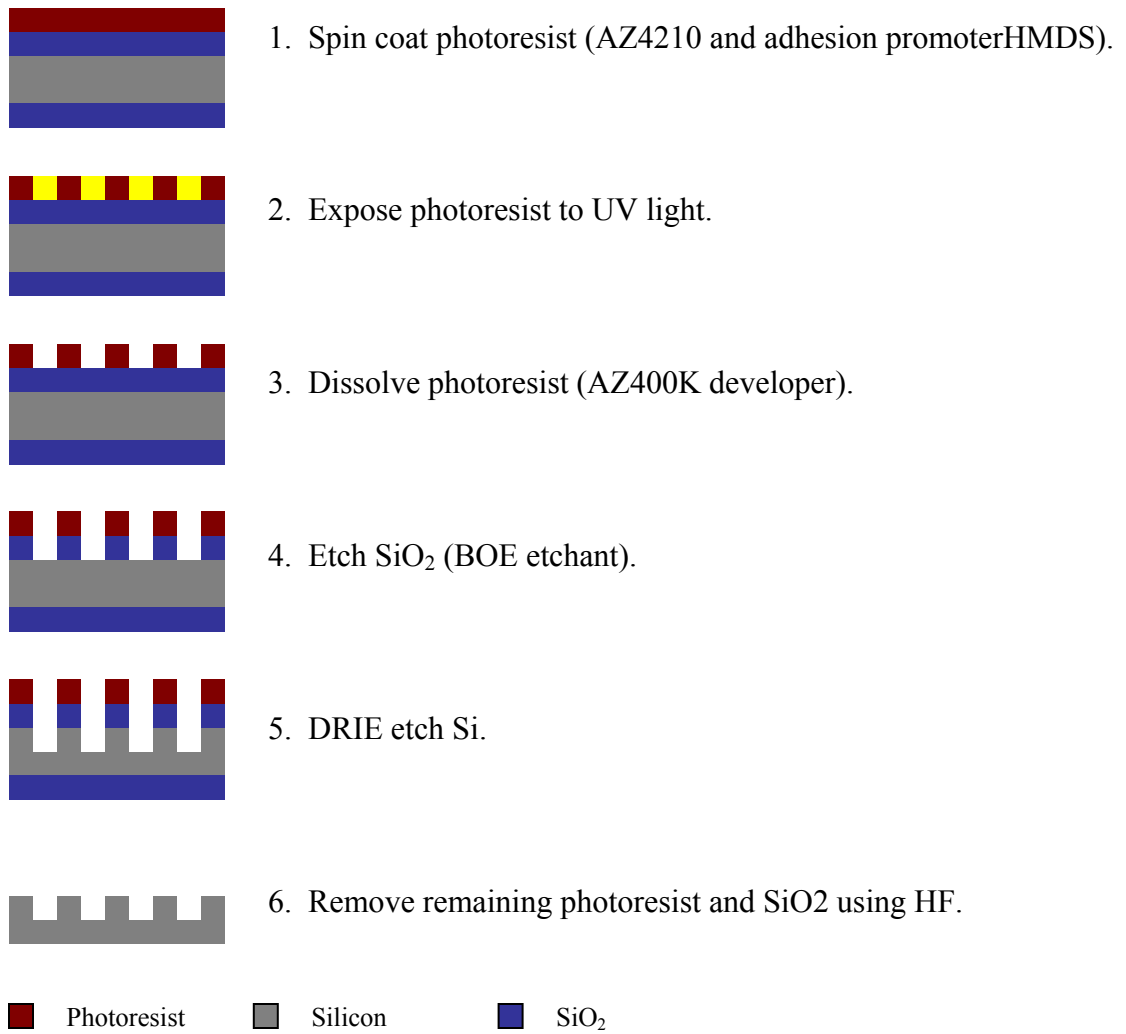


Figure 15. Microfabrication Procedure.

3.2 MICROREACTOR CHIPS

An etched reactor chip can be seen in Figure 16. Each reactor was etched to a depth of 250 μm where the width of the inlets are approximately 350 μm , the reactor channel is approximately 1mm, the length of inlet channels are approximately 20 mm and the length of reactor channel is 32 mm. Nozzle sizes are approximately 175 μm . The roughness seen in Figure 16 is simply a result of the roughness on the mask. A different mask was purchased and this roughness of the channels was eliminated. The new mask was able to achieve better resolution due to the increased dpi value of the mask printer.

Initially a thermocouple channel was incorporated into the microreactor wafer. Since we wanted to get an accurate temperature reading having the thermocouple close to the channel was important; however, it was noticed that the thermocouple channel would disappear during the developing process. Because we were unable to create a thermocouple channel extremely close to the reactor channel, a different method was used to measure the temperature in the reactor channel.

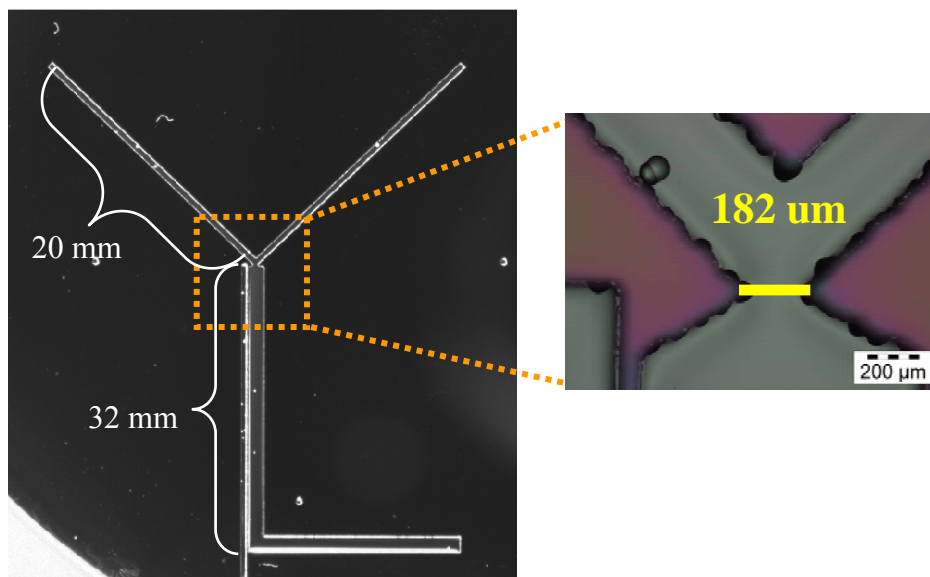


Figure 16. Image of microreactor.

3.3 CATALYST

Catalyst incorporation is a significant issue when developing a microreactor setup. Some of the most common ways to introduce the catalyst into the microreactor is to use powders, thin films produced by chemical vapor deposition (CVD), or solution methods (eg. sol-gel). The powders are not a good choice for catalysts because they cannot be added to the channel easily, they clog and cause increased pressure drops. The thin film created by CVD is not a viable option because these films are expensive to produce and once the films are deposited, the reactor cannot be reused. The best option would be a solution method because of the ease of the deposition and the thickness can be controlled based on the number of depositions. Initially, a very inexpensive solution-based method was used which did not allow for the reuse of the reactor; however it was switched out for a Pt thin foil. The Pt thin foil allowed for the reuse of the silicon wafer after

reaction, provided a specific surface area, and can be easily replaced after the catalyst is spent. The catalyst used was a 0.025 mm thick Pt foil (AlfaAesar, Pure 99.9%) which was cut to microchannel size.

3.4 REACTOR HOUSING/SETUP

The reactor setup can be seen in Figure 17. The microchannel is defined by the channel that is formed by stacking two silicon chips together. The top wafer has three drilled holes which match up to the two inlets and one outlet of the microchannel as seen in Figure 16. The two separate inlets are provided to ensure that the hydrogen and oxidant were not mixed prior to entering the channel. The two wafers are held together by pressing the two wafers between a ceramic housing, which ensures a gas tight enclosure by using Kalrez® o-rings. This ceramic housing (Macor ®) was chosen because of the ease of machinability and its high temperature stability. Two stainless steel tubes are sealed into the ceramic using a fire resistant silicone sealant. These tubes use Swagelok connections which provide an easy connection point to our standard laboratory equipment (Agilent micro GC 3000).

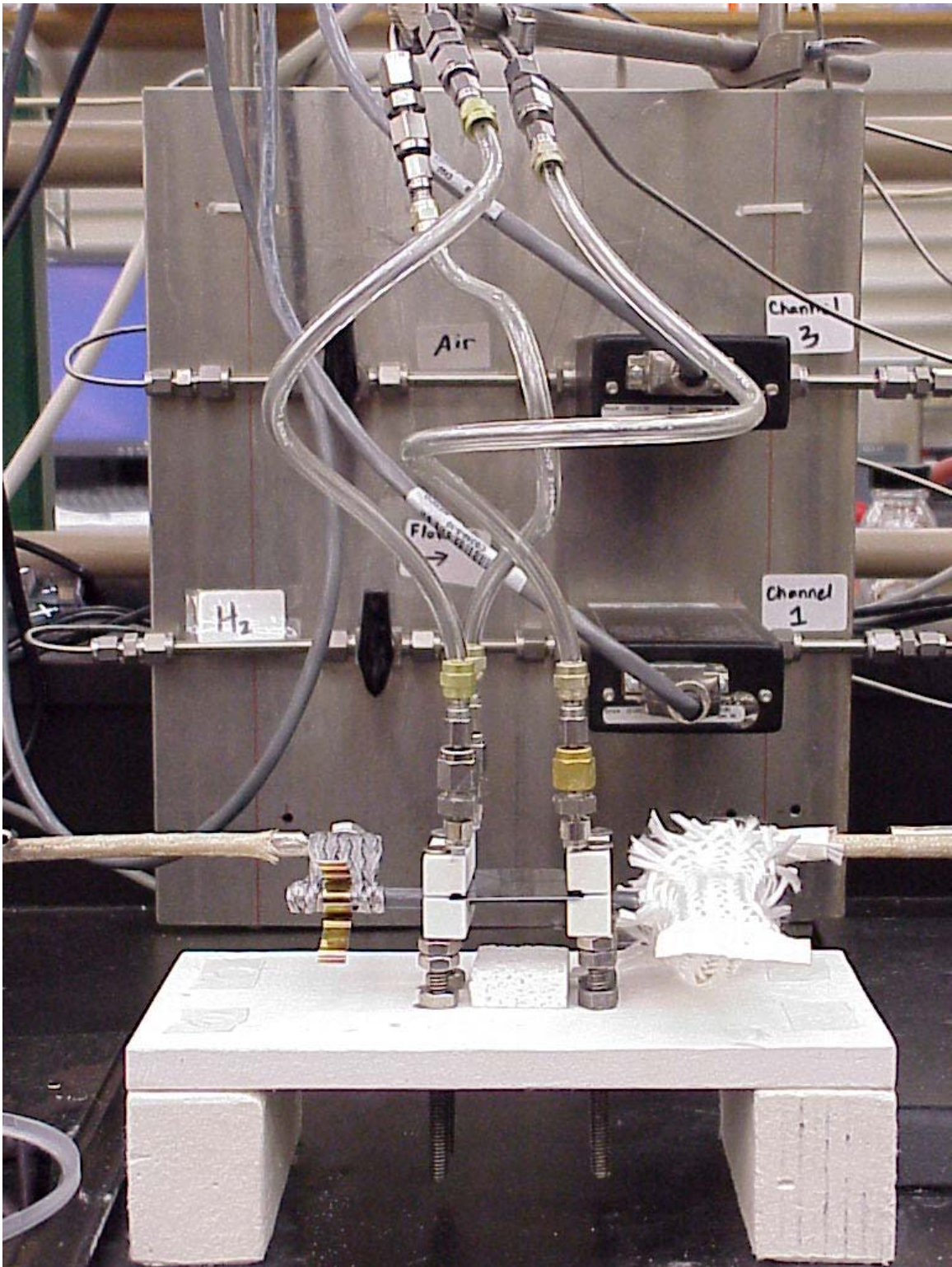


Figure 17. Experimental Setup.

3.5 EXPERIMENTAL MEASUREMENTS

To test the reaction system, the platinum foil was incorporated into the reaction channel. The reaction gases are fed through the two separate stainless steel tubing lines using two mass flow controllers (179A Mass-Flo® General Purpose Mass Flow Controller, MKS instruments). The feed gases are kept separate until they reach the nozzle, which can be seen in Figure 16. Since the mixing does not occur until the beginning of the catalyst zone, it helps to prevent homogeneous reactions between the reactants in the inlet tubing which would cause a problem in the future once the reactor can achieve higher temperatures. The reactor is heated from the bottom using a resistance heater made of molybdenum disilicide (MHI Inc). The temperature is controlled by varying the power output of the transformer using a controller provided by MHI. The temperature was measured using a K infrared thermocouple (VARIO-ZOOM™ Model 5000.2ZH, Everest Interscience). The temperature was measured over the entire reactor using a raster setup. A grid was setup to get the best resolution of the temperature without too many points. The effluent gases were analyzed by the microGC. To investigate the reaction, the conversion was calculated using Equation 25 as seen in Appendix B.

3.6 HYDROGEN/AIR

The initial mixture that was used was hydrogen and air. Initially the catalyst that was used in this case was a Pt thin film produced by depositing a 0.007 M Pt in 25% HF solution on the silicon wafer. This catalyst is deposited by a proposed method which etches away the naturally formed silicon oxide and replaces it with platinum. Several different ratios of hydrogen to air were tested

at a total flowrate of 20 sccm. Two different temperature regimes were tested: room temperature and the heater temperature of 500 degrees Celsius which corresponds to a heater power output of 55%. The 55% power output was chosen because above this power output the o-rings began to melt.

One of the temperature profiles from a mixture of hydrogen and air at 55% power output can be seen in Figure 18. A background temperature profile was measured to determine how the temperature varied from the temperature profile created from the heater and can be seen in Figure 19. From this highly exothermic reaction we would expect to see a temperature rise greater than what was seen. Because nitrogen acted as a diluent and decreased the adiabatic temperature increase, the system was switched to using hydrogen and pure oxygen.

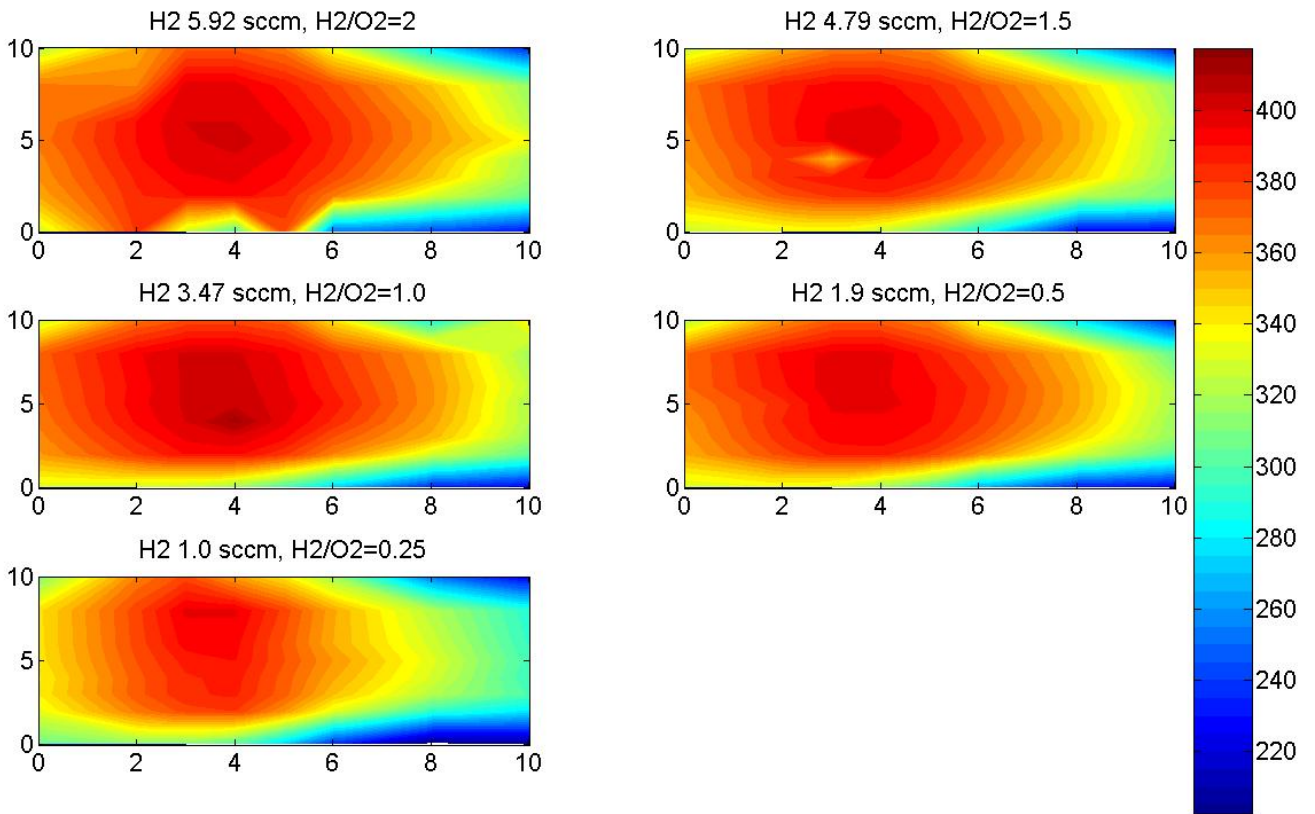


Figure 18. Contour plot of temperate raster using hydrogen/air at a power output of 55% at different hydrogen to oxygen ratios at a total flowrate of 20 sccm.

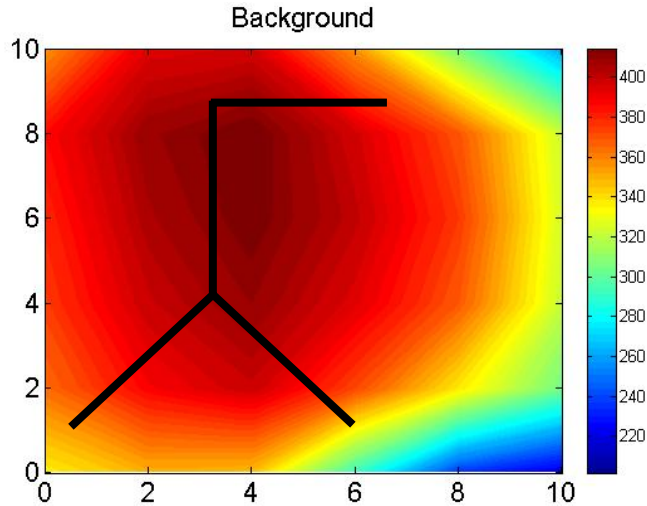


Figure 19. Contour plot of background temperature profile which corresponds to a power output of 55% and no flow.

3.7 HYDROGEN/OXYGEN

3.7.1 Premixed

Because there had been no significant temperature increase and the reaction did not seem to be occurring (no water in outlet) premixed hydrogen and oxygen was fed into the reactor. The catalyst was also changed to the platinum foil which would guarantee ample reaction sites, ensure that a reaction would occur at any temperature, and also allow for the reuse of the microreactor.

One of the temperature profiles from running premixed hydrogen and oxygen at 55% power output can be seen in Figure 20. Again the temperature profiles do not show any

significant increase in temperatures; however it was seen in the effluent stream that water was being formed.

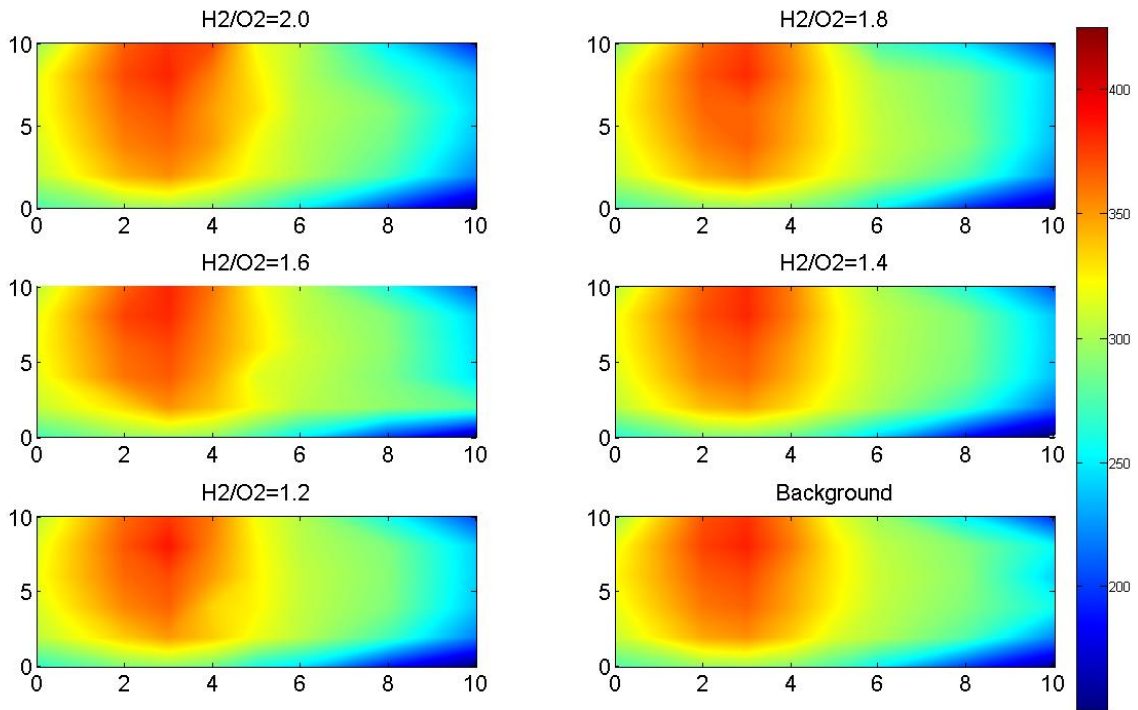


Figure 20. Contour plot of temperature raster using hydrogen/oxygen at a power output of 55% at different hydrogen to oxygen ratios at a total flowrate of 20 sccm.

From the GC measurements, the conversion was calculated using Equation 25 from Appendix B for the range of hydrogen to oxygen ratios tested. This can be seen in Figure 21. It can be seen that the conversion is highest for the stoichiometric ratio of hydrogen and oxygen.

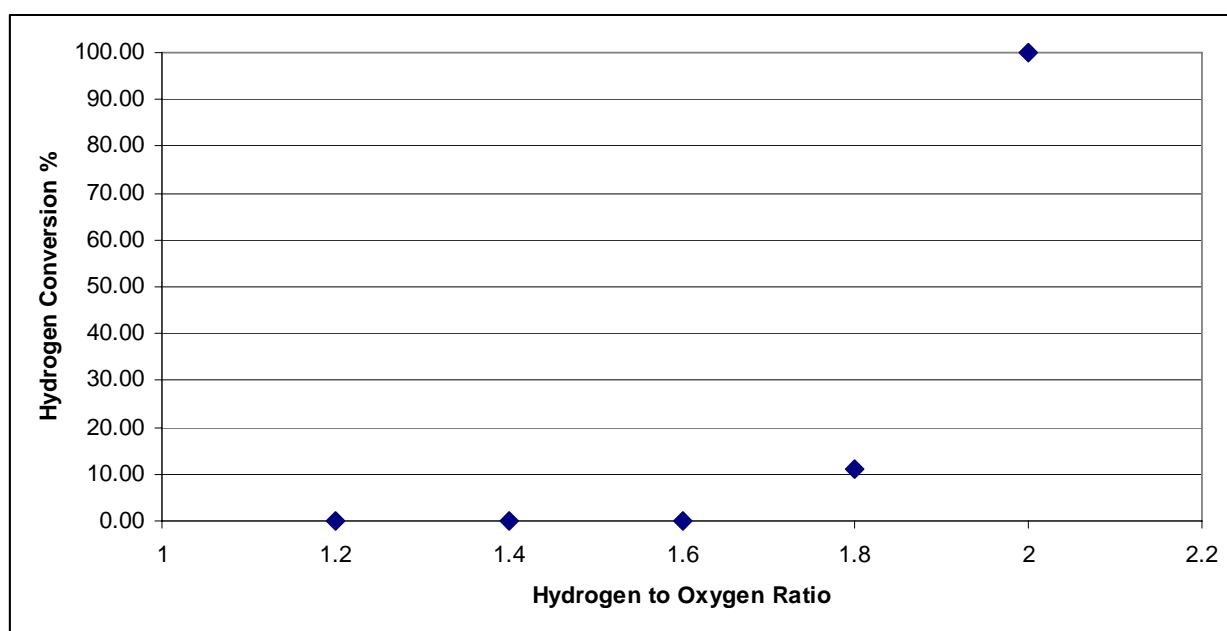


Figure 21. Conversion plot at different hydrogen to oxygen ratios at a total flowrate of 20 sccm at a power output of 55%.

To determine if the reaction front would shift inside the reactor, it was necessary to change the flowrates within the reactor. The flowrates were changed from 5-25 sccm, which are the limits of the currently installed mass flow controllers. It was expected that the reaction front would shift based on the flowrate and would be indicated by a change in the contours of the temperature; however, as it can be seen in Figure 22, the flowrates did not significantly change the position of the reaction front.

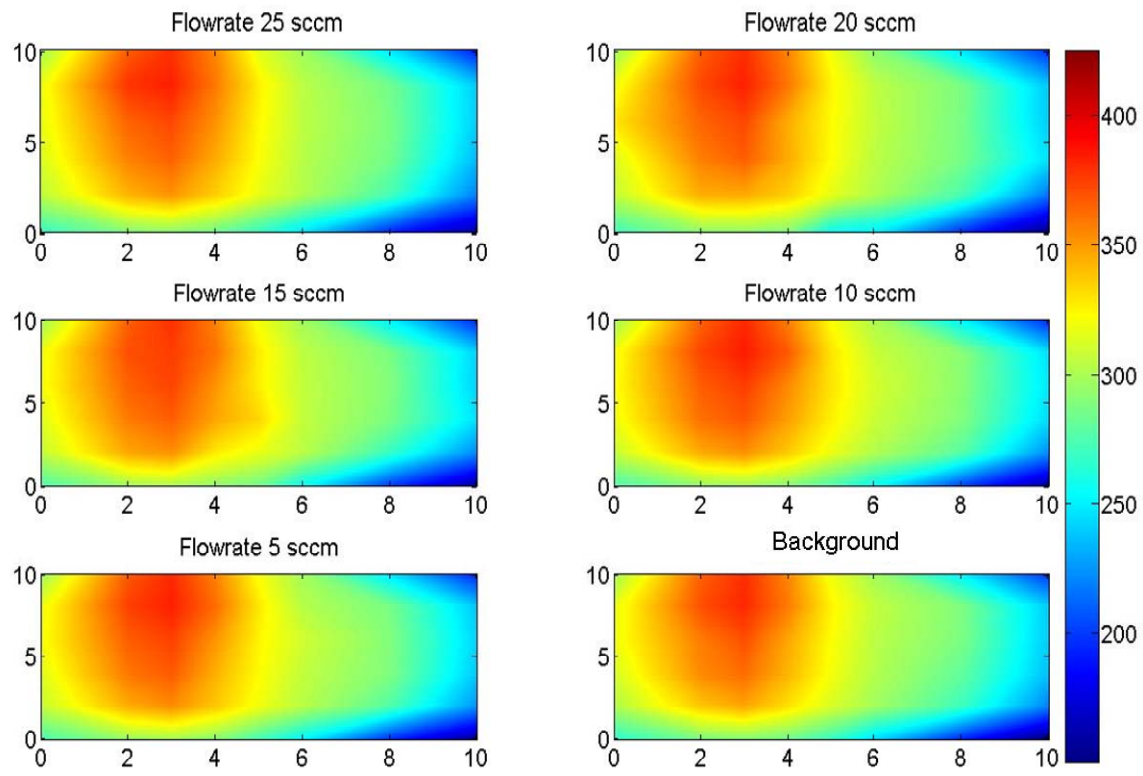


Figure 22. Contour plot of temperate raster using hydrogen/oxygen at a power output of 55% at different flowrates keeping the hydrogen/oxygen ratio of 2.0.

3.7.2 Conclusions

It was found that the reaction occurs in the microreactor when the gases are mixed outside of the reactor; however, it is definitely necessary to test the reactor in a non-premixed case. Several changes have to be made to the reactor to achieve the ultimate goal of having a high temperature modular microreactor. A few of these changes will be discussed in Section 4: Future and Outlook.

4.0 FUTURE AND OUTLOOK

There are several aspects of the modeling and experimental microreactor development that need to be addressed. First would be to increase the complexity of the model and to reduce the amount of time necessary to solve the model of the microreactor. In terms of the experimental microreactor development there are several changes that need to be made to the current experimental setup.

4.1 NUMERICAL SIMULATIONS

Since we are attempting to increase the complexity of the simulations, the focus of the future and outlook of numerical simulations will be based on Fluent. Since only the homogeneous reactions were included into the model, it is important to include the surface reactions and see quenching behavior in complex geometries. To create a more realistic model, heat transfer must be incorporated into the model. Heat transfer would need to be tested to see if it worsens the non-homogeneity of the reaction in the microchannel. With the added influence of heterogeneous reactions and heat transport, the computational demand will be increased and it would be beneficial to examine whether or not two dimensional simulations in Fluent can achieve the same accuracy in these microreactor geometries. With the switch to two dimensions not only will the simulations be shorter but the initial geometry meshing will also be less time consuming.

4.2 EXPERIMENTAL

Experimentally there are several changes that can be made here not only for the ease of use but to improve the reactor's operation. One issue that was seen was the absence of significant heat generated from the reactor which is expected from the hydrogen oxidation reaction. This could be due to the fact that the reactor is a large heat sink or that not enough heat is generated by the reaction. To increase the heat production, a larger flowrate should be used. This can be accomplished by creating a larger reactor volume, an example of this can be seen in Figure 23. This larger reactor would still consist of two inlets and one outlet, similar to the setup before; however, these inlets would then be connected to a set of diffusers which would split the one stream into several streams to increase the contact area between the two inlet streams. These streams would be fed into a large reaction channel where the catalyst would be incorporated.

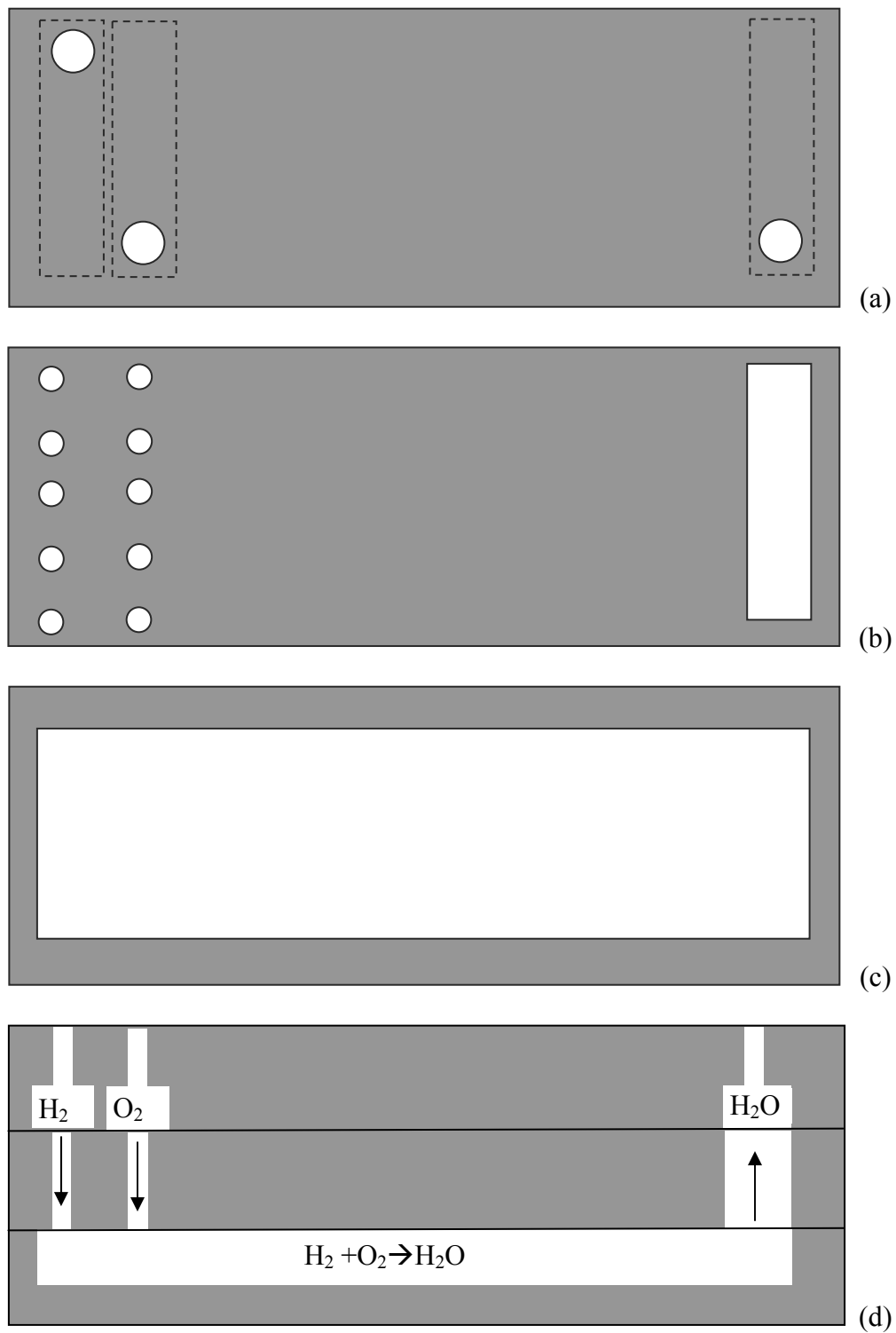


Figure 23. Proposed re-design of reactor (a-c) top view (d) side view.

Another one of the problems with the reactor is that the reactor cannot handle extreme temperatures which are necessary to study the homogeneous reaction quenching. These improvements would require a change in the overall design of the reactor. Previously designed high temperature reactors have many things in common. First, they use high temperature materials and have good heat transport. Many of these reactors have resistive heating from both sides. Suggestions for improvements on the current microreactor design are listed below:

1. Seals should be made of high temperature material (eg. gold, mica, glass).
 - a. Gold would be a good choice due to its high temperature stability which has been shown by Metzler et al [48]. In order to incorporate these orings into the current setup a better way to compress the system must be developed. Both the Si wafer and Macor can handle the compression of 200 psi [correspondence with IB Moore Representative]; however, this cannot be achieved in the current setup without cracking the silicon reactor.
 - b. The use of mica has been shown in solid oxide fuel cells and may be a useful alternative for seals [49]. They have been shown to be effective up to temperatures 700 degrees Celsius. Again the problem would arise of having proper compression on these seals.
 - c. Glass seals have been shown to be effective to temperatures up to 700 degrees Celsius because silicon and glass have low thermal mismatch up to 700 degrees Celsius [50].

Because most seals won't seal beyond a certain temperature, it will be important to keep the heating localized, which can be achieved through resistive heating. The use of thin film

platinum and high doped polysilicon has been shown to be effective resistive heaters and sensors. Platinum can be used as a heater up to about 650 degrees Celsius at which point degradation of the platinum thin film occurs [14]. Highly doped poly silicon which was passivated with silicon nitride was shown to work up to 950 degrees Celsius.

APPENDIX A

MODEL DESCRIPTION & DETAILED KINETICS

The model used was the CRESLAF model from Chemkin 4.0. The model allows for the flow to be coupled with gas phase and surface chemistry in laminar flow channels. The limitations of the model are that the model can only be used when there is a dominant flow direction and that it is two dimensional. In this model the effects of radial diffusion are simulated; however, axial diffusion is considered negligible. The boundary layer equations are derived from the general conservation equations. However, they are simplified for a two dimensional system. The boundary layer approximation is a simplification of the Navier Stokes equations. These equations become easier to solve because they become parabolic instead of elliptical and the computational efficiency is increased. The boundary layer model equations from Chemkin are listed in Table 7. The Navier Stokes equations which are solved in Fluent are listed in Table 8.

Table 7. Governing equations of the boundary layer model [42]

Momentum Balance:

$$\rho u \cdot \frac{\partial u}{\partial x} - \frac{\rho u}{M} \left(\xi \cdot \frac{dM}{dx} - \frac{dM_l}{dx} \right) \frac{\partial u}{\partial \xi} + \frac{dp}{dx} = \frac{\rho u}{M^2} \cdot \frac{\partial}{\partial \xi} \left(\rho u \mu y^{2\alpha} \cdot \frac{\partial u}{\partial \xi} \right) + g \cdot (\rho_i - \rho) \quad 4$$

Species Balance:

$$\rho u \cdot \frac{\partial Y_k}{\partial x} - \frac{\rho u}{M} \left(\xi \cdot \frac{dM}{dx} - \frac{dM_l}{dx} \right) \frac{\partial Y_k}{\partial \xi} = \dot{\omega}_k W_k - \frac{\rho u}{M} \cdot \frac{\partial}{\partial \xi} \left(y^\alpha \cdot \rho Y_k V_{k,y} \right) \quad (k = 1, \dots, K_g) \quad 5$$

Energy Balance:

$$\rho u c_p \cdot \frac{\partial T}{\partial x} - \frac{\rho u c_p}{M} \cdot \left(\xi \cdot \frac{dM}{dx} - \frac{dM_l}{dx} \right) \frac{dT}{d\xi} = \frac{\rho u}{M^2} \cdot \frac{\partial}{\partial \xi} \left(\rho u \lambda y^{2\alpha} \cdot \frac{\partial T}{\partial \xi} \right) - \sum_{k=1}^{K_g} \dot{\omega}_k W_k h_k - \frac{\rho^2 u y^\alpha}{M} \sum_{k=1}^K Y_k V_{k,y} c_{p,k} \cdot \frac{\partial T}{\partial \xi} \quad 6$$

State equation [Ideal gas law]:

$$P = \rho RT / \bar{W} \quad 7$$

Table 8. Governing equations of the Navier Stokes model [43].

Momentum Balance:

$$\frac{\partial}{\partial t}(\rho \vec{v}) + \nabla \cdot (\rho \vec{v} \vec{v}) = -\nabla p + \nabla \cdot (\overline{\tau}) + \rho \vec{g} + \vec{F} \quad \mathbf{8}$$

Continuity (Mass Balance):

$$\frac{\partial \rho}{\partial t} + \nabla \cdot (\rho \vec{v}) = S_m \quad \mathbf{9}$$

Species Balance:

$$\frac{\partial}{\partial t}(\rho Y_i) + \nabla \cdot (\rho \vec{v} Y_i) = -\nabla \cdot \vec{J}_i + R_i + S_i \quad \mathbf{10}$$

Energy Balance:

$$\frac{\partial}{\partial t}(\rho E) + \nabla \cdot (\vec{v}(\rho E + p)) = \nabla \cdot \left(k_{eff} \nabla T - \sum_j h_j J_j + (\overline{\tau_{eff}} + \vec{v}) \right) + S_h \quad \mathbf{11}$$

State equation [Ideal gas law]:

$$P = \rho RT / \overline{W} \quad \mathbf{12}$$

Table 9. Gas phase kinetics for H₂-O₂ Connaire [44].

No.	Reactions	k ₀ [mol,cm,s]	β	E [cal/mol]
1.	$\dot{\text{H}} + \text{O}_2 \leftrightarrow \dot{\text{O}} + \dot{\text{O}}\text{H}$	1.91 x 10 ¹⁴	0.00	16.44
2.	$\dot{\text{O}} + \text{H}_2 \leftrightarrow \dot{\text{H}} + \dot{\text{O}}\text{H}$	5.08 x 10 ⁴	2.67	6.292
3.	$\dot{\text{O}}\text{H} + \text{H}_2 \leftrightarrow \dot{\text{H}} + \text{H}_2\text{O}$	2.16 x 10 ⁸	1.51	3.43
4.	$\dot{\text{O}} + \text{H}_2\text{O} \leftrightarrow \dot{\text{O}}\text{H} + \dot{\text{O}}\text{H}$	2.97 x 10 ⁶	2.02	13.4
5. ^a	$\text{H}_2 + \text{M} \leftrightarrow \dot{\text{H}} + \dot{\text{H}} + \text{M}$	4.57 x 10 ¹⁹	-1.40	105.1
6. ^b	$\dot{\text{O}} + \dot{\text{O}} + \text{M} \leftrightarrow \text{O}_2 + \text{M}$	6.17 x 10 ¹⁵	-0.50	0.00
7. ^c	$\dot{\text{O}} + \dot{\text{H}} + \text{M} \leftrightarrow \dot{\text{O}}\text{H} + \text{M}$	4.72 x 10 ¹⁸	-1.00	0.00
8. ^{d,e}	$\dot{\text{H}} + \dot{\text{O}}\text{H} + \text{M} \leftrightarrow \text{H}_2\text{O} + \text{M}$	4.5 x 10 ²²	-2.00	0.00
9. ^{f,g}	$\dot{\text{H}} + \text{O}_2 + \text{M} \leftrightarrow \text{H}\dot{\text{O}}_2 + \text{M}$	3.48 x 10 ¹⁶	-0.41	-1.12
	$\dot{\text{H}} + \text{O}_2 \leftrightarrow \text{H}\dot{\text{O}}_2$	1.48 x 10 ¹²	0.60	0.00
10.	$\text{H}\dot{\text{O}}_2 + \dot{\text{H}} \leftrightarrow \text{H}_2 + \text{O}_2$	1.66 x 10 ¹³	0.00	0.82
11.	$\text{H}\dot{\text{O}}_2 + \dot{\text{H}} \leftrightarrow \dot{\text{O}}\text{H} + \dot{\text{O}}\text{H}$	7.08 x 10 ¹³	0.00	0.30
12.	$\text{H}\dot{\text{O}}_2 + \dot{\text{O}} \leftrightarrow \dot{\text{O}}\text{H} + \text{O}_2$	3.25 x 10 ¹³	0.00	0.00
13.	$\text{H}\dot{\text{O}}_2 + \dot{\text{O}}\text{H} \leftrightarrow \text{H}_2\text{O} + \text{O}_2$	2.89 x 10 ¹³	0.00	-0.50
14. ^h	$\text{H}\dot{\text{O}}_2 + \text{H}\dot{\text{O}}_2 \leftrightarrow \text{H}_2\text{O}_2 + \text{O}_2$	4.2 x 10 ¹⁴	0.00	11.98
	$\text{H}\dot{\text{O}}_2 + \text{H}\dot{\text{O}}_2 \leftrightarrow \text{H}_2\text{O}_2 + \text{O}_2$	1.3 x 10 ¹¹	0.00	
15. ^{i,f}	$\text{H}_2\text{O}_2 + \text{M} \leftrightarrow \dot{\text{O}}\text{H} + \dot{\text{O}}\text{H} + \text{M}$	1.27 x 10 ¹⁷	0.00	-1.629
	$\text{H}_2\text{O}_2 \leftrightarrow \dot{\text{O}}\text{H} + \dot{\text{O}}\text{H}$	2.95 x 10 ¹⁴	0.00	
16.	$\text{H}_2\text{O}_2 + \dot{\text{H}} \leftrightarrow \text{H}_2\text{O} + \dot{\text{O}}\text{H}$	2.41 x 10 ¹³	0.00	45.5
17.	$\text{H}_2\text{O}_2 + \dot{\text{H}} \leftrightarrow \text{H}_2 + \text{H}\dot{\text{O}}_2$	6.03 x 10 ¹³	0.00	48.4
18.	$\text{H}_2\text{O}_2 + \dot{\text{O}} \leftrightarrow \dot{\text{O}}\text{H} + \text{H}\dot{\text{O}}_2$	9.55 x 10 ⁶	2.00	3.97
19. ^h	$\text{H}_2\text{O}_2 + \dot{\text{O}}\text{H} \leftrightarrow \text{H}_2\text{O} + \text{H}\dot{\text{O}}_2$	1.0 x 10 ¹²	0.00	0.00
	$\text{H}_2\text{O}_2 + \dot{\text{O}}\text{H} \leftrightarrow \text{H}_2\text{O} + \text{H}\dot{\text{O}}_2$	5.8 x 10 ¹⁴	0.00	9.56

a.) Efficiency factors are: H₂O = 12.0, H₂ = 2.5

b.) Efficiency factors are: H₂O = 12.0, H₂ = 2.5, Ar = 0.83, He = 0.83

c.) Efficiency factors are: H₂O = 12.0, H₂ = 2.5, Ar = 0.75, He = 0.75

d.) Original pre-exponential A factor is multiplied by a factor of two

e.) Efficiency factors are: H₂O = 12.0, H₂ = 0.73, Ar = 0.38, He = 0.38

f.) Troe parameters, reaction 9: $a = 0.5$, $T^{***} = 1.0 \times 10^{-30}$, $T^* = 1.0 \times 10^{30}$, $T^{**} = 1.0 \times 10^{100}$; reaction 15: $a = 0.5$, $T^{***} = 1.0 \times 10^{-30}$, $T^* = 1.0 \times 10^{30}$

g.) Efficiency factors are: H₂ = 1.3, H₂O = 14, Ar = 0.67, He = 0.67

h.) Reactions 14 and 19 are expressed as the sum of the two rate expressions

i.) Efficiency factors are: H₂O = 12.0, H₂ = 2.5, Ar = 0.45, He = 0.45

Table 10. Surface reaction steps and rate parameters by Aghalayam et.al [45].

No.	Reactions	k_0 [mol,cm,s]	β	E [cal/mol]
1.	$H_2 + 2PT(S) \leftrightarrow 2H(S)$	0.48		0.0
2.	$2H(S) \leftrightarrow H_2 + 2PT(S)$		9.4E+11	84.0
3.	$O_2 + PT(S) \leftrightarrow O_2(S)$	0.03		0.0
4.	$O_2(S) \leftrightarrow O_2 + PT(S)$		1.0E+13	214.2
5.	$OH + PT(S) \leftrightarrow OH(S)$	1.00		0.0
6.	$OH(S) \leftrightarrow OH + PT(S)$		1.0E+13	264.6
7.	$H_2O + PT(S) \leftrightarrow H_2O(S)$	0.75		0.0
8.	$H_2O(S) \leftrightarrow H_2O + PT(S)$		1.0E+13	42.0
9.	$H + PT(S) \leftrightarrow H(S)$	1.00		0.0
10.	$H(S) \leftrightarrow H + PT(S)$		1.0E+13	252.84
11.	$O + PT(S) \leftrightarrow O(S)$	1.00		0.0
12.	$O(S) \leftrightarrow O + PT(S)$		1.E+13	281.4
13.	$OH(S) + PT(S) \leftrightarrow O(S) + H(S)$		6.1E+11	102.48
14.	$H(S) + O(S) \leftrightarrow OH(S) + PT(S)$		1.7E+10	50.82
15.	$H_2O(S) + PT(S) \leftrightarrow H(S) + OH(S)$		1.2E+10	77.28
16.	$H(S) + OH(S) \leftrightarrow H_2O(S) + PT(S)$		3.5E+11	52.08
17.	$H_2O(S) + O(S) \leftrightarrow 2OH(S)$		1.E+11	52.92
18.	$2OH(S) \leftrightarrow H_2O(S) + O(S)$		1.E+11	79.38

For catalytic wall (Pt), the surface chemistry consists of 6 species and 18 reversible reactions and the elementary step kinetics is listed in Table 10. Aghalayam et al. developed the kinetic equations and rate parameters for platinum which are used in this study [45]. The reaction rate is calculated using

$$k = k_o T^b \exp\left(\frac{-E}{RT}\right) \quad 13$$

where k_o (sec^{-1}) and E (kJ/mol). To ensure that the surface reaction rate is in terms of ($\text{mol}/\text{cm}^2\text{sec}$) it is necessary multiply k_o with Γ^{1-m} , where m is the reaction order.

Table 11. Gas-phase kinetics of H₂ – air mixture GRI[46].

No.	Reactions	k ₀ [mol,cm,s]	β	E [cal/mol]
1.	$\dot{O} + M \leftrightarrow O_2 + M$	1.2×10^{17}	-1.0	0.0
2.	$\dot{O} + H + M \leftrightarrow \dot{O}H + M$	5.0×10^{17}	-1.0	0.0
3.	$\dot{O} + H_2 \leftrightarrow \dot{H} + \dot{O}H$	3.87×10^4	2.7	6260
4.	$\dot{O} + HO_2 \leftrightarrow \dot{O}H + O_2$	2.0×10^{13}	0.0	0.0
5.	$\dot{O} + H_2O_2 \leftrightarrow \dot{O}H + \dot{H}O_2$	9.63×10^6	2.0	4000.0
6.	$\dot{H} + O_2 + M \leftrightarrow \dot{H}O_2 + M$	2.8×10^{18}	-0.86	0.0
7.	$\dot{H} + 2O_2 \leftrightarrow \dot{H}O_2 + O_2$	2.08×10^{19}	-1.24	0.0
8.	$H + O_2 + H_2O \leftrightarrow \dot{H}O_2 + H_2O$	1.13×10^{19}	-0.76	0.0
9.	$\dot{H} + O_2 + M \leftrightarrow \dot{H}O_2 + M$	2.6×10^{19}	-1.24	0.0
10.	$\dot{H} + O_2 \leftrightarrow \dot{O}H + \dot{O}$	2.65×10^{16}	-0.6707	17041
11.	$\dot{H} + M \leftrightarrow H_2 + M$	1.0×10^8	-1.0	0.0
12.	$2H + H_2 \leftrightarrow 2H_2$	9.0×10^{16}	-0.6	0.0
13.	$2H + H_2O \leftrightarrow H_2 + H_2O$	6.0×10^{19}	-1.25	0.0
14.	$\dot{H} + \dot{O}H + M \leftrightarrow H_2O + M$	2.2×10^{22}	-2.0	0.0
15.	$\dot{H} + \dot{H}O_2 \leftrightarrow \dot{O} + H_2O$	3.92×10^{12}	0.0	671
16.	$\dot{H} + \dot{H}O_2 \leftrightarrow O_2 + H_2$	4.48×10^{13}	0.0	1068
17.	$\dot{H}O_2 + \dot{H} \leftrightarrow \dot{O}H + \dot{O}H$	8.40×10^{13}	0.0	635
18.	$H_2O_2 + \dot{H} \leftrightarrow H_2 + \dot{H}O_2$	1.21×10^7	2.0	5200
19.	$H_2O_2 + \dot{H} \leftrightarrow \dot{O}H + H_2O$	1.0×10^{13}	0.0	3600
20.	$\dot{O}H + H_2 \leftrightarrow \dot{H} + H_2O$	2.16×10^8	1.51	3430
21.	$\dot{O}H + \dot{O}H + M \leftrightarrow H_2O_2 + M$	7.40×10^{13}	-0.37	0.0
22.	$2\dot{O}H \leftrightarrow H_2O + \dot{O}$	3.57×10^4	2.4	-2110
23.	$\dot{H}O_2 + \dot{O}H \leftrightarrow H_2O + O_2$	1.45×10^{13}	0.0	-500
24.	$H_2O_2 + \dot{O}H \leftrightarrow H_2O + \dot{H}O_2$	2.0×10^{12}	0.0	427
25.	$H_2O_2 + \dot{O}H \leftrightarrow H_2O + \dot{H}O_2$	1.70×10^{18}	0.0	29410
26.	$\dot{H}O_2 + \dot{H}O_2 \leftrightarrow H_2O_2 + O_2$	1.30×10^{11}	0.0	-1630
27.	$\dot{H}O_2 + \dot{H}O_2 \leftrightarrow H_2O_2 + O_2$	4.20×10^{14}	0.0	12000
28.	$\dot{H}O_2 + \dot{O}H \leftrightarrow H_2O + O_2$	5.00×10^{15}	0.0	17330
a.)	Efficiency factors are: H ₂ O = 20.0			
b.)	Efficiency factors are: H ₂ O = 6.0, \dot{H} = 2.0, H ₂ = 3.0			
c.)	Efficiency factors are: H ₂ O = 21.0, H ₂ = 3.3, O ₂ = 0, N ₂ = 0			

A.1.1 Example Input File

```
ICRD RAD    ! Cylindrical Coordinates
MULT       ! Use Multicomponent Transport
PRES 0.986923 ! Pressure (atm)
TINL 700.0  ! Inlet Temperature (K)
TSRF 700.0  ! Surface Temperature (K)
VEL 900.0   ! Axial Velocity (cm/sec)
XTMP 1.0E-6 ! Ramp-up Distance for Surface Temperature (cm)
HITE 0.01   ! Reactor Radius (cm)
NPTS 100.0  ! Number of Grid Points
STCH 1.2    ! Stretch Parameter for Non-uniform Grid
XEND 2.00! Ending Axial Position (cm)
BULK PT(B) 1.0 ! Bulk Activity (mole fraction)
REAC H2 0.29577465 ! Reactant Fraction (mole fraction)
REAC N2 0.55633803 ! Reactant Fraction (mole fraction)
REAC O2 0.14788732 ! Reactant Fraction (mole fraction)
SURF H(S) 0.395 ! Surface Fraction (site fraction)
SURF H2O(S) 8.5E-5 ! Surface Fraction (site fraction)
SURF O(S) 0.000977 ! Surface Fraction (site fraction)
SURF OH(S) 0.000538 ! Surface Fraction (site fraction)
SURF PT(S) 0.6034 ! Surface Fraction (site fraction)
ATOL 0.0001 ! Absolute Tolerance
RTOL 0.001 ! Relative Tolerance
GFAC 1.0 ! Gas Reaction Rate Multiplier
SFAC 1.0 ! Surface Reaction Rate Multiplier
END
```

APPENDIX B

MASS BALANCES IN MICROREACTOR

The following describes how to calculate the hydrogen conversion within the reactor using the molar concentration (y_i) detected by the GC at the outlet of the microreactor.

The total flow of moles entering the system is given by:

$$\dot{N}_{in} = \dot{N}_{H_2,in} + \dot{N}_{O_2,in} \quad 14$$

The total flow of moles exiting the system and entering the GC is given by:

$$\dot{N}_{GC} = \dot{N}_{H_2,GC} + \dot{N}_{O_2,GC} + \dot{N}_{H_2O,GC} \quad 15$$

The total flow of moles exiting the system and condensing:

$$\dot{N}_{out} = \dot{N}_{H_2O,out} \quad 16$$

An atomic balance over hydrogen gives the following equations:

$$y_{H_2,in} * \dot{N}_{in} = y_{H_2,GC} * \dot{N}_{GC} + y_{H_2O,GC} * \dot{N}_{GC} + y_{H_2O,out} * \dot{N}_{out} \quad 17$$

Since generally no water is measured at the GC the equation simplifies to:

$$y_{H_2,in} * \dot{N}_{,in} = y_{H_2,GC} * \dot{N}_{GC} + y_{H_2O,out} * \dot{N}_{out} \quad 18$$

An atomic balance over oxygen gives the following equation:

$$y_{O_2,in} * \dot{N}_{,in} = y_{O_2,GC} * \dot{N}_{GC} + \frac{1}{2} y_{H_2O,GC} * \dot{N}_{GC} + \frac{1}{2} y_{H_2O,out} * \dot{N}_{out} \quad 19$$

Since generally no water is measured at the GC the equation simplifies to:

$$y_{O_2,in} * \dot{N}_{,in} = y_{O_2,GC} * \dot{N}_{GC} + \frac{1}{2} y_{H_2O,out} * \dot{N}_{out} \quad 20$$

Since the condensing stream only contains water $y_{H_2O,out}$ equals 1.

$$y_{O_2,in} * \dot{N}_{,in} = y_{O_2,GC} * \dot{N}_{GC} + \frac{1}{2} \dot{N}_{out} \quad 21$$

$$y_{H_2,in} * \dot{N}_{,in} = y_{H_2,GC} * \dot{N}_{GC} + \dot{N}_{out} \quad 22$$

Eliminating \dot{N}_{out} :

$$2 * y_{O_2,in} * \dot{N}_{,in} = 2 * y_{O_2,GC} * \dot{N}_{GC} + y_{H_2,in} * \dot{N}_{,in} - y_{H_2,GC} * \dot{N}_{GC} \quad 23$$

The hydrogen conversion is defined as:

$$X_{H_2} = \frac{\Delta \dot{N}_{H_2}}{\dot{N}_{H_2,in}} = 1 - \frac{y_{H_2,GC} * \dot{N}_{GC}}{y_{H_2,in} * \dot{N}_{,in}} \quad 24$$

From the above equation 24 and substitution of $\frac{\dot{N}_{GC}}{\dot{N}_{,in}}$:

$$X_{H_2} = 1 - \frac{y_{H_2,GC} * \dot{N}_{GC}}{y_{H_2,in} * \dot{N}_{in}} = 1 - \frac{y_{H_2,GC} * (2 * y_{O_2,in} - y_{H_2,in})}{y_{H_2,in} * (2 * y_{O_2,GC} - y_{H_2,GC})} \quad 25$$

The conversion can be calculated simply from the values obtained from the GC and also the initial conditions.

BIBLIOGRAPHY

1. Roberts, Christopher B., Elbashir, Nimir O. 2003. *Fuel Processing Technology*, **83**(1-3): 1-9.
2. Vesper, G. 2001. *Chem. Eng. Sci.*, **56** (4): 1265-1273.
3. Vesper, G., Friedrich, G., Freygang, M., Zengerle, R. 1998 *ASME-DSC* **66**: 199-206.
4. Vesper, G., Friedrich, G., Freygang, M., Zengerle, R. 1999. *Stud. Surf. Sci. Catal.* **122**: 237-246.
5. Chattopadhyay, Sudipta. Navigating Reactor Safety in Catalytic Microchannel Reactors [dissertation]. Chemical Engineering, University of Pittsburgh, 2004.
6. Lewis, B., Elbe, G.V. 1987. *Combustion and Flames and Explosions of Gases*. New York: Academic Press.
7. Vesper, G., Schmidt, L.D. 1996. *AIChE*. **42**(4): 1077-1087.
8. Vlachos, D.G. 1996. *Chem. Eng. Sci.* **51**(10): 2429-2438.
9. Enomoto et al., 1981. *Hydrogen Energy Prog.* **2**: 1149–1163.
10. Griffin, T.A., Pfefferle, L.D. 1990. *AIChE*. **36** (6): p. 861-870.
11. Mueller, M.A., Yetter, R.A., Dryer, F.L.. 1999. *Int. J. Chem. Kinetics*. **31**(10):705-724.
12. Warnatz, J., Maas, U., Dibble, R.W. 1996. *Combustion-Physical and Chemical Fundamentals, Modeling and Simulation, Experiments, Pollutant Formation*, Springer Verlag, Heidelberg, Germany.
13. Jensen, K.F. 2001. *Chem. Eng. Sci.* **56** (2): 293-303.
14. Apelee, Christine. Technologies for High-temperature Silicon Microreactors [dissertation]. Departement de Microtechnique. Ecole Polytechnique Federale de Lausanne, 2000.
15. Tonkovich, A.L.Y., Zilka, J.L., Powell, M.R., Call, C.J. 1998. *Second International Conference on Microtechnology*, New Orleans, Louisiana: 45-53.

16. Mayer, J., Fichtner, M., Wolf, D., Schubert, K. 1999. *IMRET 3*. Frankfurt, Springer Verlag: 187-196
17. Kursawe, A., Honicke, D. 2000. *IMRET 4*. Atlanta, AIChE: 153-166
18. Kestenbaum, H. et al. 1999. *IMRET 3*. Frankfurt, Springer Verlag: 207-212
19. Honicke, D., Wiessmeier, G. 1996. *Workshop on Microsystem Technology for Chemical and Biological Microreactors*, VCH Verlagsgesellschaft: 93-107
20. Lerou, J.J. et al. *Workshop on Microsystem Technology for Chemical and Biological Microreactors*, VCH Verlagsgesellschaft: 51-69
21. Zech, T., Honicke, D., Lohf, A., Golbig, K., Richter, T. *IMRET 3*. Frankfurt, Springer Verlag: 260-266
22. Zech, T., Honicke, D. 2000. *IMRET 4*. Atlanta, AIChE: 379-389.
23. Wunsch, R., Fichtner, M., Schubert, K. 1999. *IMRET 3*. Frankfurt, Springer Verlag: 625-635
24. Jensen, K. F. et al. 1997. First International Conference on Microreaction Technology, Frankfurt, Springer Verlag (Berlin): 2-9.
25. Jensen, K. F. et al. 1998. MicroTAS '98, Banff, Kluwer Academic Publishers: 463-468
26. Hsing, I.-M., et al. 1996. Solid-State Sensor and Actuator Workshop, Hilton Head, South Carolina: 15-18.
27. R. Srinivasan, et al. 1997. *Transducers '97*: 163-166.
28. R. Srinivasan, et. 1997. *AIChE*. **43**(11), 3059-3069
29. A. J. Franz et al. 1998. *Second International Conference on Microtechnology*, New Orleans, Louisiana: 33-38.
30. Franz, A. J. et al. *IMRET 3*. Frankfurt, Springer Verlag: 197-206.
31. U. Hagendorf, et al. 1998. *Second International Conference on Microtechnology*, New Orleans, Louisiana: 81-87
32. Vesper, G., Friedrich, G., Freygang, M., Zengerle, R. 1999. *MEMS 99*, Orlando, Florida: 394-399.
33. Vesper, G., Friedrich, G., Freygang, M., Zengerle, R. 1999. *IMRET 3*. Frankfurt, Springer Verlag: 674-686.
34. A. L. Y Tonkovich, et al. 1998. *Second International Conference on Microtechnology*, New Orleans: 186-195

35. Tonkovich, A. L. Y et al.1999. *IMRET 3*. Frankfurt, Springer Verlag: 364-371.
36. Christian, M. M., Kenis P. J. A. 2006. *Lab Chip*. 6: 1328–1337.
37. Pfeifer, P. et al .1999. *IMRET 3*. Frankfurt, Springer Verlag: 373-382.
38. S. P. Fitzgerald et al. 2000. *IMRET 4*. Atlanta, AIChE: 358-363.
39. Hessel, V. et al. 1999.*IMRET 3*. Frankfurt, Springer Verlag: 151-164.
40. Tiggelaar, R.M. et al. 2005. *Lab Chip*. 5: 326 – 336.
41. Kartavya, Jain. Design, Fabrication and Testing of a High Temperature Ceramic Microreactor for Synthesizing Silicon Nitride Nanoparticles [thesis]. Department of Industrial Engineering. Oregon State University, 2007.
42. R.J.Kee, F.M.Rupley, J.A.Miller, M.E.Coltrin, J.F.Grcar, E.Meeks, H.K.Moffat, A.E.Lutz, G.Dixon-Lewis, M.D.Smooke, J.Warnatz, G.H.Evans, R.S.Larson, R.E.Mitchell, L.R.Petzold, W.C.Reynolds, M.Caracotsios, W.E.Stewart, P.Glarborg, C.Wang, O.Adigun, W.G.Houf, C.P.Chou, S.F.Miller, P.Ho, and D.J.Young, CHEMKIN Release 4.0, Reaction Design, Inc., San Diego, CA (2004).
43. Fluent Inc. *Fluent 6.1 User's Guide*, 2003.
44. Conaire, Marcus Ó et al. 2004. *Int. J. of Chem. Kinetics*. **36**(11): 603-662
45. Aghalayam, P., Park,Y., Vlachos,D.G. 2000.*AIChE*, 46(10): 2017-2029.
46. Gregory P. Smith, David M. Golden, Michael Frenklach, Nigel W. Moriarty, Boris Eiteneer, Mikhail Goldenberg, C. Thomas Bowman, Ronald K. Hanson, Soonho Song, William C. Gardiner, Jr., Vitali V. Lissianski, and Zhiwei Qin .(October 30, 2002). *GRI Mech 3.0*. [Retrieved] August 20, 2004, [from]http://www.me.berkeley.edu/gri_mech/
47. Choudhury, P. R.,ed. 1997. *Handbook of microlithography, micromachining, and Microfabrication: Voume 1*. Bellingham, Washington, The Society of Photo-Optical Instrumentation Engineer Press.
48. Younes-Metzler, O. et al. 2005. *Applied Catalysis A: General*. **284**(1-2): 5-10.
49. Fergus, J. W. 2005. *Journal of Power Sources*. 147 (1-2): 46-57.
50. Peles, Yoav et al. 2004. *Journal of Microelectromechanical systems*.13(1): 31-40.